CHAPTER 4

Loss-of-Function Analyses Defines Vital and Redundant Functions of the *Plasmodium* Rhomboid Protease Family

Jing-wen Lin[1], Patrícia Meireles[2], Miguel Prudêncio[2], Sabine Engelmann[3], Takeshi Annoura[1], Mohammed Sajid[1], Séverine Chevalley-Maurel[1], Jai Ramesar[1], Carolin Nahar[4], Cristina M.C. Avramut[5], Abraham J. Koster[5], Kai Matuschewski[3, 4], Andrew P. Waters[6], Chris J. Janse[1], Gunnar R. Mair[7], Shahid M. Khan[1]

[1]Leiden Malaria Research Group (Parasitology); [5]Section Electron Microscopy (Molecular Cell Biology), Leiden University Medical Centre, Leiden, The Netherlands

[2]Malaria Unit, [7]Molecular Parasitology Unit, Instituto de Medicina Molecular, Faculdade de Medicina, Universidade de Lisboa, Lisboa, Portugal

[3]Parasitology, Department of Infectious Diseases, University of Heidelberg Medical School, Heidelberg, Germany

[4]Max Planck Institute for Infection Biology, Parasitology Unit, Berlin, Germany

[6]Division of Infection and Immunity, Institute of Biomedical Life Sciences & Wellcome Centre for Molecular Parasitology, Glasgow Biomedical Research Centre, University of Glasgow, Glasgow, Scotland

Molecular Microbiology 2013, 88(2): 318–338.

Abstract

Rhomboid-like proteases cleave membrane-anchored proteins within their transmembrane domains. In apicomplexan parasites substrates include molecules that function in parasite motility and host cell invasion. While two *Plasmodium* rhomboids, ROM1 and ROM4, have been examined, the roles of the remaining six rhomboids during the malaria parasite's life cycle are unknown. We present systematic gene deletion analyses of all eight *Plasmodium* rhomboid-like proteins as a means to discover stage-specific phenotypes and potential functions in the rodent malaria model, *P. berghei*. Four rhomboids (ROM4, 6, 7 and 8) are refractory to gene deletion, suggesting an essential role during asexual blood-stage development. In contrast ROM1, 3, 9 and 10 were dispensable for blood stage development and exhibited no, subtle or severe defects in mosquito or liver development. Parasites lacking ROM9 and ROM10 showed no major phenotypic defects. Parasites lacking ROM1 presented a delay in blood stage patency following liver infection, but in contrast to a previous study blood stage parasites had similar growth and virulence characteristics as wild type parasites. Parasites lacking ROM3 in mosquitoes readily established oocysts but failed to produce sporozoites. ROM3 is the first apicomplexan rhomboid identified to play a vital role in sporogony.

Introduction

Rhomboid-like proteins are intramembrane serine proteases that hydrolyse a substrate within its transmembrane (TM) spanning domain [1]. The first rhomboid protease described was *Drosophila melanogaster* Rhomboid-1 that initiates cell signaling by cleaving the membrane-resident Spitz, an epidermal growth factor (EGF)-like ligand precursor, releasing it as an activated molecule from the membrane and promoting subsequent EGF-receptor signaling [2]. With the exception of viruses, rhomboid-like proteins are found in all kingdoms of life and share a conserved core structure of six TM domains that contains the catalytic serine-histidine diad [3–7]. Interestingly, as a family of proteins, they share only around 5% sequence identity in the core region [8] and have highly variable amino termini. Some members have additional TM domains at either N- or C- termini of the core six, but their precise functions are unknown. Rhomboids function in cell-cell signaling in metazoans [9,10], quorum sensing between bacteria [11], facilitate mitochondrial membrane fusion in yeast [12] and regulate apoptosis [13].

Many eukaryotic organisms contain large rhomboid gene families. Multiple rhomboid-like enzymes are also found in the genomes of apicomplexan parasites such as *Toxoplasma gondii*, *Plasmodium spp.*, *Eimeria tenella*, *Cryptosporidium spp.*, *Theileria spp.* and *Babesia bovis*. Based on a phylogenetic clustering of rhomboid-like proteins, a nomenclature has been defined according to the initial assignment of *T. gondii rhomboids* [14], which expresses six rhomboid-like proteins TgROM1–6. Only four TgROMs (i.e. ROM1, 3, 4 and 6) have direct *Plasmodium* homologs [14]; there are no direct homologs of TgROM2 and TgROM5 in *Plasmodium* and ROM7–10 are only present in *Plasmodium* but not in *T. gondii*. Although *Plasmodium* species do not have a direct TgROM5 homolog, *P. falciparum* ROM1 and ROM4 share substrate specificities with TgROM5 [15]. Apicomplexan ROM6 is most likely an evolutionarily ancient mitochondrial PARL-like rhomboid, whereas all the others seem to be unique to apicomplexan parasites [14]. Interestingly, *Plasmodium* ROM9 also has a putative mitochondrial-targeting sequence and clusters with PARL-like rhomboids [16].

Although *in vitro* certain rhomboids of apicomplexan parasites can cleave adhesins that are known to mediate recognition of, and attachment to host cells, their *in vivo* substrate specificities are largely unknown [16,17]. Understanding the biological functions of apicomplexan rhomboids is an active area of research because of the critical roles identified for several of these molecules in host cell invasion and pathogenesis [16–18]. In *T. gondii*, TgROM4 has been shown to process surface adhesins including MIC 2, 3 (microneme proteins) and apical membrane antigen 1 (AMA1 [18]); this TgROM4-mediated AMA1 cleavage critically regulates the parasite's switch from an invasive to a

replicative mode [19]. TgROM1 is localized in micronemes [20] and although it is critical for parasite growth, TgROM1 is not essential for parasite invasion [21]. From the eight *Plasmodium* rhomboids, only ROM1 and ROM4 have been analyzed in more detail. *In vitro* substrates of the *P. falciparum* proteins include the merozoite-specific proteins AMA1 and proteins of the EBL (erythrocyte binding ligands) and RBL (reticulocyte binding ligands) families as well as several proteins of the invasive ookinete- and sporozoite-stages, such as TRAP (thrombospondin-related anonymous protein), CTRP (circumsporozoite- and TRAP-related protein) and MAEBL (merozoite adhesive erythrocytic binding protein) [15]. Structural analysis of the RBL protein EBA175 (Erythrocyte-binding antigen 175) and TRAP provided evidence for shedding of these proteins by a rhomboid-like protease [22] and indeed both proteins are cleaved *in vitro* by ROM4 [22,23]. In *P. falciparum* only a small fraction of AMA1 is shed by ROM1 and the intramembrane cleavage can be reduced to undetectable levels by mutagenesis without discernible phenotypic consequences [24]. The successful generation of *P. berghei* and *P. yoelii* mutants that lack expression of ROM1 also demonstrated that ROM1 is not essential for blood stage multiplication [25,26]. Blood stages of these mutants suffer only from a minor reduction in growth, again indicating that intramembrane cleavage of AMA1 by ROM1 is not essential for invasion of erythrocytes. ROM1 mutants in *P. yoelii* also showed a slight growth defect during liver stage development which has been attributed to reduced cleavage of the parasitophorous vacuole protein UIS4 (upregulated in sporozoites 4) by ROM1 [26]. Whether additional proteins are processed by *Plasmodium* ROM4 or ROM1 *in vivo* is still unknown. The non-essential nature of ROM1 during the complete lifecycle indicates that other rhomboids or proteases from other families can cleave substrates of ROM1. ROM4 on the other hand has been reported to be essential for blood stage growth as attempts to mutate the *rom4* gene of *P. falciparum* failed [22]. However, differences in cellular localization and *in vitro* substrate specificities of ROM1 and ROM4 [15,22] raise questions as to whether these rhomboids cleave the same substrates *in vivo*. In blood stage *P. falciparum* ROM1 is located in micronemes of merozoites and ROM4 is embedded into the merozoite plasma membrane [22].

Due to the absence of data defining *Plasmodium* rhomboid expression, cellular localization, or importance during the parasite's life cycle, it is largely unknown which, if any rhomboids are biologically essential, redundant or perhaps share overlapping functions. We therefore undertook a genetic screen of all 8 rhomboids by targeting each gene for deletion by homologous recombination using the genetically most tractable malaria parasite, *P. berghei*. Multiple attempts to disrupt genes encoding ROM4, ROM6, ROM7 and ROM8 failed, suggesting that these proteins have essential, non-redundant functions during blood stage development. We show that in addition to ROM1, three

other rhomboid-like proteases – ROM3, ROM9 and ROM10 – are redundant for asexual blood stage development in mice. Parasites lacking ROM9 and ROM10 showed no major phenotypic defects during the entire life cycle; however parasites lacking ROM1 were slightly compromised with respect to their ability to develop in the liver. Although already transcribed strongly in the female gametocyte, ROM3 is crucial during oocyst development inside the mosquito. Parasites lacking ROM3 produce normal numbers of ookinetes that readily establish oocysts in the mosquito. Although normal in size and number, oocysts fail to sporulate, suggesting that ROM3 plays a key role in the regulation of cytokinesis and production of individual sporozoites.

Results

The gene expression profiles of rhomboids across the parasite life cycle

The genome of the rodent malaria parasite *P. berghei* contains eight genes encoding rhomboid proteases [14] (Gene IDs are shown in Table 1) Each member shows a high level of sequence identity (70–85%) with its rhomboid ortholog from the human malaria parasite *P. falciparum* and shares a syntenic location in the genome (www.plasmodb.org) with an identical exon/intron gene structure.

We compared expression data of all rhomboid genes in *P. berghei* and *P. falciparum* in publicly available literature as well as transcriptome and proteome datasets across the life cycle (Table 1) (www.plasmodb.org and [27]). Immunofluorescence assays (IFA) on HA-tagged ROM1 and ROM4 show expression of these proteins in dividing schizonts and merozoites in *P. falciparum* [22]. A similar pattern of expression of *P. berghei* and *P. yoelii* ROM1 has been shown in schizonts and merozoites by IFA [25–26]. In both *P. berghei* and *P. falciparum* ROM1 is located in the micronemes. *P. berghei* ROM1 and ROM4 of *P. falciparum* and *P. berghei* have been detected in the sporozoite stage [25, 23] (Table 1). Our RT-PCR analyses (Fig. S1) demonstrate transcription of *P. berghei rom1* and *rom4* in blood stages and sporozoites. These different observations indicate that both ROM1 and ROM4 of human and rodent parasites have comparable patterns of expression and cellular location. For other rhomboids the information on stage-specific expression is much more limited. Proteome analyses indicate that ROM6, ROM9 and ROM10 are expressed in *P. falciparum* gametocytes (Table 1); however, proteome evidence for expression of these proteins in *P. berghei* gametocytes or other blood stages is absent. ROM7 and ROM8 are absent in all *P. falciparum* and *P. berghei* proteomes and ROM3 is only detected in *P. falciparum* blood stages. EST, RNAseq (Table 1) and RT-PCR analyses (Fig. S1), however, indicate that ROM3, ROM7 and ROM8 are expressed in blood stages and therefore the

absence in proteomes may suggest that rhomboids are relatively low abundant proteins, although we have to take into account the difficulties of proteomic sequencing multi-pass transmembrane proteins. *P. falciparum* RNAseq analyses indicate that transcription of *rom3* and *rom4* is upregulated in gametocytes compared to asexual stages (Table 1). RNAseq analyses of different *P. berghei* blood stages also showed strongly increased transcripts levels of *rom3* and *rom4* in gametocytes (W.A.M. Hoeijmakers, A. Religa, C.J. Janse, A.P. Waters, & H.G. Stunnenberg, unpublished data). We confirmed transcription of these rhomboids in *P. berghei* gametocytes by RT-PCR (Fig. S1).

The similarities between the eight rhomboid genes of *P. falciparum* and *P. berghei* and similarities in expression patterns and cellular locations of several rhomboids point towards a conserved function between rhomboid orthologs across the parasites' life-cycle in both species. Since most rhomboids appear to be expressed in multiple life cycle stages, the expression pattern is however not a good indicator for a putative role at a distinct life cycle stage.

Table 1. Expression profile of *Plasmodium rhomboids*

Protein	Gene ID	mRNA				Protein			
P. berghei		**As[1,2]**	**Gct[1,2]**	**Ook[1]**	**Sp[1,2]**	**As[3]**	**Gct[4]**		**Sp[3]**
ROM1	PBANKA_093350	+ (-)	+ (-)	++	+ (++)	- (+[5])	±		- (+[5])
ROM3	PBANKA_070270	- (++)	+ (-)	-	- (-)	-	-		-
ROM4	PBANKA_110650	+ (++)	+ (-)	++	+ (++)	- (+[6])	-		- (+[6])
ROM6	PBANKA_135810	+ (-)	+ (-)	-	- (+)	-	-		-
ROM7	PBANKA_113460	+ (-)	- (-)	-	- (+)	-	-		-
ROM8	PBANKA_103130	+ (-)	- (-)	-	- (-)	-	-		-
ROM9	PBANKA_111470	± (-)	± (-)	-	+ (-)	-	-		-
ROM10	PBANKA_111780	+ (++)	± (-)	+	- (-)	-	-		-
P. falciparum		**As[7]**	**Gct[7]**		**Sp[8]**	**As[3]**	**Gct[3]**	**Ooc[3]**	**Sp[3]**
ROM1	PF3D7_1114100	+	±		+	+	-	-	-
ROM3	PF3D7_0828000	±	++		+	±	-	-	-
ROM4	PF3D7_0506900	+	++		+	++	-	-	+
ROM6	PF3D7_1345200	±	±		+	-	±	-	-
ROM7	PF3D7_1358300	±	-		-	-	-	-	-
ROM8	PF3D7_1411200	+	+		+	-	-	-	-
ROM9	PF3D7_0515100	±	±		+	-	±	-	-
ROM10	PF3D7_0618600	+	±		+	±	+	-	-

AS, asexual stages; Gct, gametocytes; Ook, ookinetes; Ooc, oocysts; Sp, sporozoites
[1] RT-PCR results in this study (see Figure S1)
[2] (PlasmoDB EST data in parentheses: - = no data; + = 1 EST; ++ = 2-7 ESTs)
[3] PlasmoDB proteome data (- = no data; ±=1-2; +=3-10; ++=>10)
[4] PbANKA Male vs female gametocyte proteome (Khan *et al*, 2005)
[5] IFA evidence using anti-PbROM1 serum (Srinivasan *et al*, 2009)
[6] Western and IFA evidence using anti-PbROM4 serum (Ejigiri I *et al*, 2012)
[7] PlasmoDB RNAseq data (- = no data; ± = 0-6; + = 6-10) RPKM (log2)
[8] PlasmoDB oligo array (- = no data; ± = 1-100; + = 100-1000; ++ > 1000) RMA value

Evidence for an essential role of ROM4, 6, 7 and 8 in asexual blood stage parasites – ROM1, 3, 9 and 10 are dispensable.

As a first step towards understanding the roles of rhomboid proteases during the *Plasmodium* life cycle, we undertook a systematic, individual gene deletion approach for each of the eight *P. berghei* rhomboid genes and provide here a detailed analysis of the growth characteristics of gene deletion mutants for four rhomboids. Using well-established standard assays, the following phenotypes of the gene deletion mutants were characterized throughout the complete life cycle including blood, mosquito and liver stages: *in vivo* asexual blood stage multiplication rate, *in vivo* gametocyte production, *in vitro* ookinete formation, oocyst and sporozoite development in *A. stephensi* mosquitoes and the prepatent period in mice after injection of sporozoites. The prepatent period is defined as the time taken to achieve a 0.5–2% blood stage parasitemia in mice after intravenous inoculation of 10^4 sporozoites.

Standard genetic modification technologies used to replace entire *rhomboid* genes by double cross-over integration with a drug resistant marker resulted in gene deletion mutants for *rom1*, *3*, *9* and *10*, while multiple attempts to disrupt *rom4*, *6*, *7* and *8* were unsuccessful (see Table S1, S2 and S3 for details of these unsuccessful gene-deletion attempts including primers used to amplify the targeting sequences, generate the gene-deletion constructs and genotype). We demonstrated by RT-PCR that *rom4*, *6*, *7* and *8* are transcribed in blood stages (Fig. S1) and the multiple unsuccessful attempts to disrupt *rom4*, *6*, *7* and *8* may indicate that these genes have a critical function for asexual blood stage growth and multiplication. While a failure to disrupt a gene is not an unequivocal proof that the encoded protein is essential for blood stage growth/multiplication for *rom4* we show that the failure of disruption is not due to refractoriness of the genetic locus to genetic modification by creating a transgenic mutant (*rom4::mCherry*) that expresses a C-terminally mCherry-tagged ROM4 (Fig. S2). Genotype analysis of the *rom4::mCherry* parasites and analysis of ROM4::mCherry expression (Fig. S2) demonstrates that correct genetic modification of the *rom4* locus is possible. Immunofluorescence analysis of ROM4::mCherry revealed its expression in gametocytes (Fig. S2); however, the very weak fluorescence signals in asexual blood stages prevented confirmation of merozoite surface location observed in *P. falciparum* (Fig. S2). The normal asexual multiplication rate (Table 2) indicates that the mCherry-tagged ROM4 functions normally during blood stage development. All information on the failed attempts to disrupt *rom4*, *6*, *7* and *8*, including DNA constructs and primers have been submitted to the RMgmDB database of genetically modified rodent malaria parasites (www.pberghei.eu).

The correct integration of the constructs and successful disruption of the other

rhomboids, *rom1*, *3*, *9* and *10*, were confirmed by diagnostic PCR and Southern analysis of separated chromosomes (Figs. 1 and 2). Northern analyses showed transcription of all four genes in blood stages of wild type *P. berghei* ANKA parasites and confirmed the lack of transcription in the blood stages of the respective gene-deletion mutants (Figs. 1 and 2). The clonal lines of the gene-deletion mutants Δ*rom1*, Δ*rom3*, Δ*rom9* and Δ*rom10* showed no change in asexual growth rates *in vivo* (Table 2). Despite the evidence for transcription and protein expression of ROM1, 9 and 10 in asexual blood stages (Figs. 1, 2 and S1; Table 1), this indicates a non-essential, redundant function for these proteins during asexual blood stage multiplication.

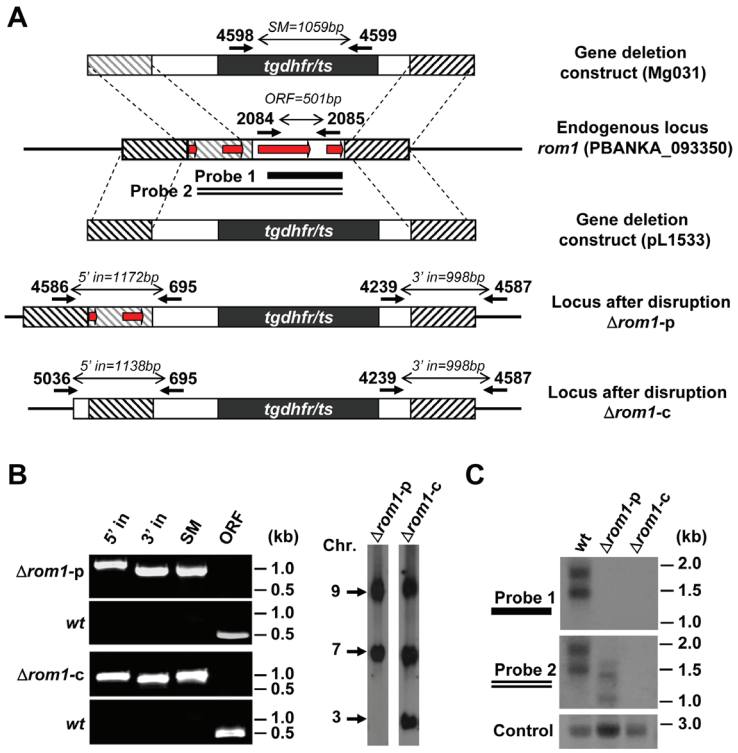

Figure 1. Generation of mutants lacking expression of *P. berghei* rhomboid 1.

A. Schematic representation of the constructs Mg031 and pL1533 targeting *rhomboid-1* for gene deletion by double cross-over homologous recombination at the target regions (hatched boxes), and the locus before and after disruption. Each construct contains the *tgdhfr/ts* selection cassette (black box). Mg031 replaces the 3rd and 4th exons (red arrows) of the open reading frame (ORF) but retains 1st and 2nd exons in mutant Δ*rom1*-p. pL1533 replaces the complete ORF in Δ*rom1*-c. Primer positions for diagnostic PCRs, amplicon sizes and the location of two PCR probes for the Northern blot analyses are shown (see Table S3 for primer sequences).

B. Diagnostic PCRs (left) and Southern analyses of separated chromosomes (right) confirm the correct

integration of the constructs in Δ*rom1*-p and Δ*rom1*-c. Primer pairs and amplicon sizes are shown in **A**: 5'/3' in, integration PCR; SM, amplification of the *tgdhfr*/*ts* selection cassette; ORF, deleted ORF. For Southern analyses, pulsed field gel-separated chromosomes were hybridized with a 3'UTR *pbdhfr* probe that recognizes the constructs integrated into *rom1* locus on chromosome 9 and the endogenous *dhfr*/*ts* locus on chromosome 7; in the Δ*rom1*-c line, the probe also hybridizes to the GFP-luciferase reporter cassette in the *230p* locus on chromosome 3.

C. Northern blot analyses of mRNA from mixed blood stage parasites confirm the loss of wild type *rom1* transcripts in Δ*rom1*-p and Δ*rom1*-c. Locations of the PCR probes used for hybridization were shown in **A** (PCR probes were generated by PCR-amplification from wild type *P. berghei* genomic DNA using primers 2084/2085 for Probe 1, and primers 2082/2085 for Probe 2; see Table S3 for primer sequences). In blood stages of Δ*rom1*-p, truncated transcripts were detected with Probe 2, recognizing exons 1 and 2 of *rom1*. In Δ*rom1*-c, no transcripts were detected. As a loading control, hybridization was performed with probe L644R that recognizes the large subunit ribosomal RNA. wt, wild-type *P. berghei* ANKA.

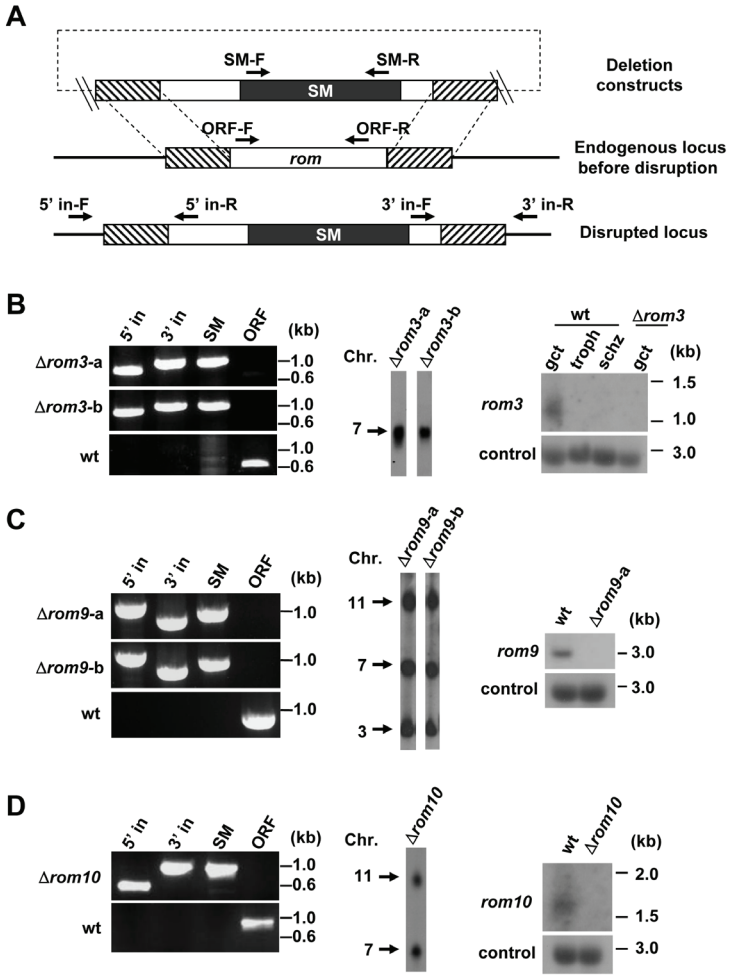

Figure 2. Generation of mutants lacking expression of *P. berghei* rhomboid 3, 9 and 10

A. Schematic representation of the DNA construct used for targeting rhomboid genes for deletion and the gene locus before and after disruption. The constructs which contain a drug-selectable marker cassette (SM; black box) disrupt the genes by double cross-over homologous recombination at the target regions (hatched boxes). The locations of primers for diagnostic PCRs are shown.

B. Diagnostic PCRs, Southern and Northern analyses confirm correct disruption of *rhomboid 3* (*rom3*) in 2 independent mutants, Δ*rom3*-a and Δ*rom3*-b. For diagnostic PCRs (left), the following primers were used: 5' integration (5' in): 2389/695; 3' integration: (3' in) 4239/1886; amplification of the *tgdhfr*/*ts* selection cassette (SM): 4598/4599; deleted ORF (ORF): 1812/1813. For Southern analyses of separated chromosomes (middle), pulsed field gel-separated chromosome were hybridized using a *tgdhfr*/*ts* probe that recognizes the construct integrated into *rom3* locus on chromosome 7. Northern blot analysis (right) of mRNA of different blood stages shows transcripts only present in wild type gametocytes (gct). No transcripts are detected in trophozoites (troph) or schizonts (schz). The analysis also confirms the loss of *rom3* transcripts in gct of Δ*rom3*. Hybridization was performed using a PCR probe recognizing *rom3* ORF (primers 1812/1813). As a loading control, hybridization was performed with probe L644R that recognizes the large subunit ribosomal RNA.

C. Analysis of two independent mutants, Δ*rom9*-a and Δ*rom9*-b, lacking expression of ROM9. For diagnostic PCRs (left), the following primers were used: 5' in: 7083/4906; 3' in: 4239/7084; SM (h*dfhr*::y*fcu*): 4698/4699; ORF: 7085/7086. For Southern analyses (middle), chromosomes were hybridized using a 3'UTR *pbdhfr* probe that recognizes the construct integrated into *rom9* on chromosome 11, the *dhfr*/*ts* on chromosome 7 and the GFP-luciferase reporter cassette in the *230p* locus on chromosome 3. Northern blot was hybridized with a PCR probe recognizing *rom9* ORF (primers 7085/7086) (right).

D. Analysis of Δ*rom10* lacking expression of ROM10. For diagnostic PCRs (left), the following primers were used: 5' in: 6939/4179; 3' in: 4239/2088; SM (*tgdhfr*/*ts*): 4598/4599; ORF: 6940/2066. Chromosomes were hybridized using a 3'UTR *pbdhfr* probe that recognizes the construct integrated into *rom10* on chromosome 11 and the *dhfr*/*ts* on chromosome 7 (middle). Northern blot was hybridized with a PCR probe recognizing *rom10* ORF (primers 6940/2066) (right). See Table S3 for all primer sequences and product sizes.

ROM9 and ROM10 are dispensable for the entire life cycle

Two independent gene-deletion mutants were generated for *rom9*: Δ*rom9*-a and Δ*rom9*-b (Fig. 2C). Asexual blood stage multiplication, gametocyte production and ookinete production of both Δ*rom9* mutants were similar to that of wild type *P. berghei* parasites.

We analyzed Δ*rom9*-a parasites during development in mosquitoes and in hepatocytes. The Δ*rom9* parasites produced wild type levels of oocysts (Table 2). Although we showed that *rom9* is transcribed in salivary gland sporozoites (Fig. S1), we found no significant differences between Δ*rom9* parasites and wild type parasites with respect to the production of sporozoites, their gliding motility (data not shown), traversal and invasion of hepatocytes and in the prepatent period in mice after injection of sporozoites (Table 2). Immunofluorescence analyses of liver stage parasites stained with antibodies against markers for parasite development (HSP70), parasitophorous vacuole membrane (UIS4 and EXP1) and merozoite formation (MSP1), also revealed no distinct differences in morphology between Δ*rom9* and wild type liver stage parasites at 24h or 48h after sporozoite invasion (Fig. 3 A). However, Δ*rom9* parasite loads between 53 and 57 hours after infection (measured by RT-PCR, FACS and luciferase assay) were consistently lower both *in vitro* and *in vivo* (Fig. 3 B&C) which may indicate that this enzyme plays a (minor)

Table 2. Phenotypes of *P. berghei* mutants lacking expression of rhomboids

Lines	Asexual multiplication rate[1] (s.d.)	Gametocyte production[2] % (s.d.)	Ookinete production[3] % (s.d.)	Oocyst production[4] (s.d.)	Sporozoite production[5] × 10^3 (s.d.)	Sporozoite traversal[6] % (s.d.)	Sporozoite invasion rate[7] % (s.d.)	Prepatent period compare to wt[8]
Mutants								
Δ*rom1*-p	10 (0) n= 2	16.4 (0.5)	56.6 (1.8)	156.3 (151.8)	ND	ND	ND	ND
Δ*rom1*-c	10 (0) n= 3	17.3 (1.0)	68.9 (9.5)	155.6 (118.9)	35.9 (3.3)	27.3 (7.6)	23.3 (8.5) *	+1 (n=3)
				220.0 (70.3)	49.0 (1.6)	ND	35.6 (10.6) *	+1 (n=3)
				ND	ND	ND	58.5 (6.8)	ND
Δ*rom3*-a	10 (0) n= 3	17.9 (1.3)	61.3 (5.9)	148.4 (136.8)	NA	NA	NA	NA
Δ*rom3*-b	10 (0) n= 2	18.9 (3.0)	71.0 (6.1)	259.7 (155.8)	NA	NA	NA	NA
Δ*rom9*-a	10 (0) n= 4	18.9 (4.1)	74.3 (11.0)	145.8 (123.8)	43.2 (6.5)	21.1 (2.1)	51.7 (9.2)	+0 (n=5)
Δ*rom9*-b	10 (0) n= 4	19.0 (2,7)	74.2 (4.6)	ND	ND	ND	ND	ND
Δ*rom10*	10 (0) n= 4	18.1 (2.6)	63.8 (7.4)	191.8 (147.2)	44.7 (8.0)	ND	53.3 (4.5)	+0 (n=3)
Tagging mutants								
rom3::gfp	10 (0) n= 3	18.0 (2.7)	66.5 (4.7)	298.2 (110.7)	51.4 (8.9)	ND	ND	ND
rom4::mCherry	10 (0) n= 7	ND	ND	ND	ND	ND	ND	ND
wt[9]	10 (0) n>10	15-25	50-90	120-290	35-80	19.3-25.7	53.0 -61.8	+0

[1] The multiplication rate per 24 hour of blood stage parasites in mice infected with a single parasite;
[2] The percentage of blood stage parasites developing into gametocytes *in vivo*;
[3] The percentage of female gametes developing into mature ookinetes *in vitro*;
[4] The mean number of oocysts per mosquito (day 11–14);
[5] The mean number of salivary gland sporozoites per mosquito (day 19–22);
[6] Percentage of Dextran positive cells in Huh7 cell cultures 2h after post infection;
[7] The percentage of intracellular sporozoites at 3 h post infection of Huh7 cell cultures;
[8] The prepatent period (measured in days post sporozoite infection) is defined as the day when a blood stage infection with a parasitemia of 0.5–2% is observed. (+0 = similar to wild type; +1 = 1 day delay compared to wild type;
[9] The developmental data for wild type parasites are shown as the range of mean values of > 10 experiments.
ND, not done; NA, not applicable.
* P<0.05, determined by student T-test as compared to wild type control run in parallel

role during liver stage development.

We generated one gene deletion mutant for *rom10* and analyzed this mutant throughout the entire life cycle. The phenotype of Δ*rom10* parasites was similar to that of wild type parasites in all developmental assays (Table 2), specifically *in vivo* asexual multiplication rate, *in vivo* gametocyte production, *in vitro* ookinete production, oocyst and sporozoite production and *in vivo* liver stage development. In addition, Δ*rom10* sporozoites showed normal rates of gliding (data not shown), *in vitro* hepatocyte invasion rate and prepatent period (Table 2). These results indicate that this protein is redundant and/or that its function can be fulfilled by other (rhomboid) proteases.

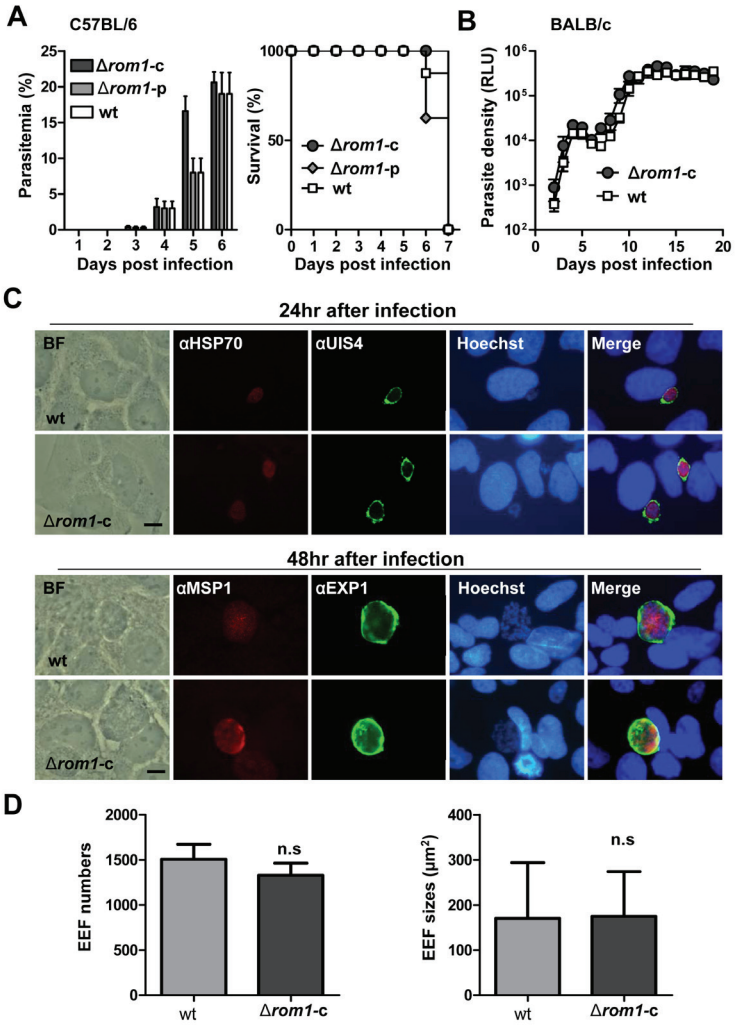

Figure 3. Liver stage development of Δ*rom9* parasites

A. Immunofluorescence assays of liver stages of Δ*rom9* and the wild type (wt) control *Pb*GFP-Luc$_{schz}$ at 24h and 48h after sporozoite infection of cultured Huh7 cells show a comparable morphology of Δ*rom9* and wild type parasites. Anti-HSP70 (red) antibody highlights the parasite's cytoplasm while anti-UIS4 (green) antibody decorates the parasitophorous vacuole membrane (PVM). Anti-MSP1 (red) antibody recognizes developing merozoites and anti-EXP1 (green) antibody the PVM. Nuclei were stained with Hoechst-33342 (Blue). BF, bright field; scale bars equals 10µm.

B. Parasite loads at 57h in cultured Huh7 cells after infection with 5×10^4 Δ*rom9* or wild type control *Pb*GFP-Luc$_{schz}$ sporozoites as determined by luciferase assay (left), qRT-PCR (middle) and FACS (right). All assays show a slight reduction of mutant parasite loads, however, only the relative infection value determined by qRT-PCR shows significant reduction (student T-test: n.s: not significant; *: P<0.5).

C. Parasite loads in C57BL/6 mice at 53h after injection of 1×10^4 Δ*rom9* sporozoites or wild type control *Pb*GFP-Luc$_{schz}$ sporozoites as determined by *in vivo* imaging (left and middle) and qRT-PCR (right). Representative rainbow images of luminescence in livers of live mice (left) and the corresponding luminescence levels (photons/sec) of livers in whole mice (middle) are shown (student T-test: n.s: not significant). The lines indicate mean values and the error bars indicate standard deviations.

Δ*rom1* parasites have wild type blood-stage growth and virulence characteristics, but show delayed liver stage development

In the course of this study we generated two independent *P. berghei* Δ*rom1* mutants; the first mutant Δ*rom1*-p is a partial gene deletion lacking the 3rd and 4th exons of *rom1* that contain the catalytic diad (Fig. 1A&B); the second mutant Δ*rom1*-c lacks the entire open reading frame (Fig. 1A&B). Northern analyses of *rom1* transcripts in blood stages using two PCR-amplified probes specific to 3rd and 4th exons, or to the whole ORF, showed that Δ*rom1*-p lacks transcripts containing the 3rd and 4th exons but still produces stable, truncated transcripts consisting of the 1st and 2nd exons. As expected, Δ*rom1*-c had no detectable *rom1* transcripts (Fig. 1C). Both Δ*rom1*-p and Δ*rom1*-c showed *in vivo* multiplication rates were similar to wild type *P. berghei* parasites when analyzed in the cloning-assay (Table 2). To determine possible differences in growth rate and virulence during prolonged infections in mice, we analyzed the growth rate of Δ*rom1* and wild type parasites in C57BL/6 and in BALB/c mice (Fig. 4A&B). C57BL/6 mice are sensitive to experimental cerebral malaria (ECM) and cerebral complications develop 6–8 days post-infection with *P. berghei* ANKA parasites, whereas BALB/c mice are ECM-resistant and develop fulminating (and lethal) parasitemias peaking 2–3 weeks after infection. In both C57BL/6 and BALB/c mice Δ*rom1* parasites showed infection patterns that were highly similar to infections initiated with wild parasites (Fig. 4A&B); all Δ*rom1* infected C57BL/6 mice developed ECM symptoms at day 6 or 7 after infection (Fig. 4A).

Δ*rom1* parasites were next examined during mosquito and liver stage development. These parasites produced numbers of ookinetes, oocysts and salivary gland sporozoites similar to those of wild type parasites (Table 2). However, liver-stage development was reduced as shown by a 1-day extension of the prepatent period in mice following the inoculation

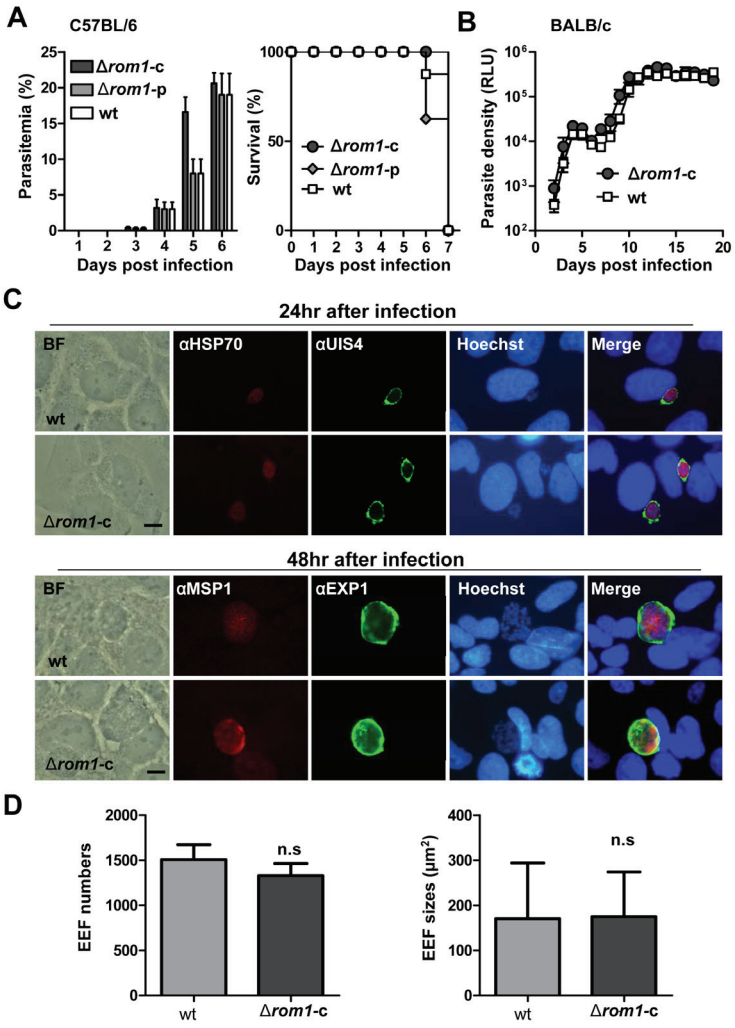

Figure 4. Blood and liver stage development of Δ*rom1* parasites.

A. The course of infection (left panel) and survival curve (right panel) in C57BL/6 mice (n=6) infected with 10^5 wild-type (wt, cl15cy1), Δ*rom1*-p or Δ*rom1*-c. The parasitemia developed in mice infected with wt, Δ*rom1*-p and Δ*rom1*-c parasites are highly comparable during the whole course of infection (left). All C57BL/6 mice infected with wild-type (wt, cl15cy1), Δ*rom1*-p and Δ*rom1*-c parasites developed ECM complications on day 6–7 as indicated by a drop in body temperature below 34°C; mice were sacrificed at this point (right).

B. The course of infection in BALB/c mice (n=6) infected with 10^4 parasites of wild-type (wt, GPF-luc$_{con}$) or Δ*rom1*-c parasites. Parasite densities were determined by measuring luciferase activity indicated as relative light unit (RLU) in the IVDL-assay. Error bars indicate standard deviations in A and B.

C. Immunofluorescence analyses of Δ*rom1*-c and the wild type (wt, GFP-Luc$_{con}$) exo-erythrocytic forms (EEF) at 24h and 48h after infection with 1×10^4 Δ*rom1*-c or wild type (GFP-Luc$_{con}$) parasites show normal development of Δ*rom1*-c parasites compared to wild type control. Anti-HSP70 (red) and anti-UIS4 (green) antibodies recognize the parasite's cytoplasm and the parasitophorous vacuole membrane (PVM). Anti-MSP1 (red) antibodies recognize developing merozoites and anti-EXP1 (green) antibodies stain the PVM. Nuclei were stained with

Hoechst-33342 (Blue). BF, bright field; scale bars equals 10µm.

D. EEF numbers per well of cultured Huh7 cells at 24hr (left) and the sizes of EEFs at 48hr (right) after sporozoite infection. The numbers of EEFs were determined by counting anti-UIS4 staining positive EEFs in the immunofluorescence assay, and the EEF sizes were determined by measuring the sizes of anti-Hsp70 staining positive parasites. The lines indicate mean values and the error bars indicate standard deviations.

with 10^4 purified sporozoites. While gliding motility (data not shown) and the rate of cell traversal of sporozoites were similar to wild type parasites (Table 2), we observed in two out of three experiments a reduction in sporozoite *in vitro* invasion rates (Table 2) that could explain (in part) the delay in the prepatent period. Immunofluorescence analyses of liver stage parasites stained with antibodies against markers for parasite development (HSP70), PVM (UIS4 and EXP1) and merozoite formation (MSP1), revealed no distinct differences in morphology and size between Δ*rom1* and wild type liver stages at 24h or 48h after sporozoite invasion (Fig. 4C). Although a significant reduction in parasite loads and expression of UIS4 have been reported for liver stages of *P. yoelii* mutants lacking expression of ROM1 [26], we only observed a slight, but not significant, reduction in numbers of liver stages as determined by anti-UIS4 antibody staining (Fig. 4D) and we did not observe that these mutants had unusual PVM morphology. Liver stages of Δ*rom1* and wild-type parasites were also comparable in size at 48 hrs post infection (Fig. 4D).

Δ*rom3* parasites establish oocysts but fail to produce sporozoites

Two independent gene-deletion mutants, Δ*rom3*-a and Δ*rom3*-b, were generated (Fig. 2B). Asexual blood stage multiplication rates of both mutants determined in the cloning assay were normal and Δ*rom3* parasites produced wild type levels of gametocytes, ookinetes and oocysts (Table 2). By light microscopy, Δ*rom3* ookinetes have the characteristics of fully mature wild-type ookinetes such as an elongated 'banana' shape, hemozoin clusters and a centrally located, enlarged nucleus and the Δ*rom3* and wild type ookinetes show a similar (tetraploid) DNA content (Fig. S3). In addition, by electron microscopy analyses we were unable to detect differences in the ultrastructural morphology of wild-type and Δ*rom3* ookinetes; with respect to the nucleus, crystalloid body and the structure of the apical complex (Fig. S5). All membranes of these organelles exhibit a normal structure and the apical complex of Δ*rom3* ookinetes had the characteristic features of abundant micronemes, and the presence of microtubules and the inner membrane complex.

However, no sporozoites were detected in salivary glands of mosquitoes infected with Δ*rom3*-a or Δ*rom3*-b in three independent experiments. Inspection of Δ*rom3* oocysts by light-microscopy revealed normal oocyst production but a complete absence of sporozoite formation; mature oocysts had clearly vacuolated cytoplasm and there were no signs

of sporulation (Fig. 5A). Western analysis of circumsporozoite protein (CSP) expression using anti-CSP antibody in oocysts-containing midguts at day 10 after infection, showed that CSP is almost absent in the Δ*rom3* oocysts (Fig. 5B). An indirect immunofluorescence assay (IFA) on wild type and Δ*rom3* oocysts confirmed the strongly reduced CSP levels in Δ*rom3* oocysts (Fig. 5C). There was also reduced intensity of Hoechst DNA-staining indicating decreased DNA replication in these oocysts (Fig. 5C). The crucial role of ROM3 in oocyst maturation/sporogony is unexpected given the high transcript levels detected in gametocytes (Table 1, Fig. S1B). When we analyzed ROM3::GFP expression in *rom3*::*gfp* parasites (with the endogenous *rom3* C-terminally tagged with GFP), we observed GFP signal in all female gametocytes (but not in male gametocytes) that persisted into mature ookinetes but was undetectable in oocysts (day 6-17) and sporozoites (Fig. 5D).

The normal development throughout the life cycle (Fig. 5D, Table 2) indicates that the C-terminal GFP-tag does not affect the essential function of ROM3 during sporozoite formation. We attempted to use the *rom3*::*gfp* parasites to gain a better understanding of the localization of ROM3 in female gametocytes and ookinetes. Specifically, we extracted soluble and insoluble protein fractions of *rom3*::*gfp* gametocytes and ookinetes and then examined the presence of ROM3 protein using antibodies against the GFP tag. Unfortunately, we were unable to unambiguously identify ROM::GFP in either fraction, presumably due to the very low expression of ROM3 in these stages (data not shown).

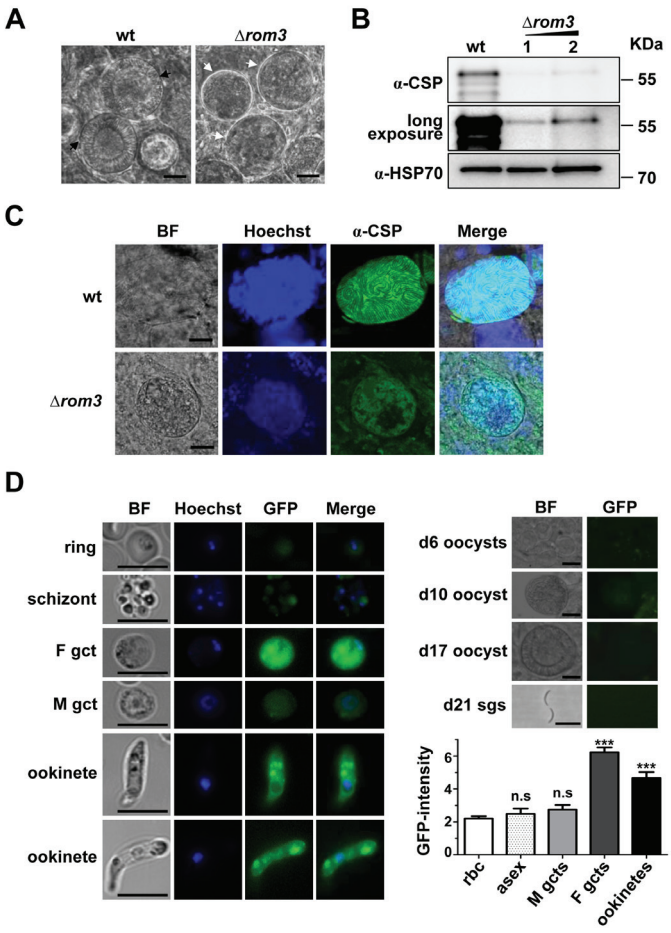

Figure 5. Rhomboid 3 is essential for sporozoite formation in oocysts.

A. Phase contrast microscopy of wild type and aberrant, vacuolated Δ*rom3* oocysts on day 12 after mosquito infection. Mutants lack any signs of sporozoite formation (white arrow) whereas wild type (wt) oocysts collected on the same day show clear sporulation (black arrow). Scale bar 10 µm.

B. Western blot analysis of midguts from infected mosquitoes. Midguts from mosquitoes infected with Δ*rom3* (1 or 2 midguts, day 10) and wild-type (wt, day 10) were separated on SDS-PAGE and stained with anti-CSP and anti-HSP70 antibodies. A longer exposure of the anti-CSP blot is also shown.

C. Developmental defects of Δ*rom3* parasites examined by immunofluorescence assays. Compared to wild-type (wt), Δ*rom3* oocyst show decreased CSP expression as shown by staining oocysts with anti-CSP (green) antibody and reduced staining with the DNA-specific dye Hoechst-33342 (blue), indicating less DNA replication. BF, bright field. Scale bar 10 µm.

D. All *rom3::gfp* female gametocytes (F gct; n=50) and ookinetes (n >100) exhibited a GFP signal that was significantly above background values (***P<0.0001, student T-test). No GFP signals above background were detected in either male gametocyte (M gct; n=30) or asexual blood stages. In the mosquito vector no GFP signals were detected in either *rom3::gfp* oocysts (6-17 days after mosquito infection) or in salivary gland sporozoites (sgs, day 21). Nuclei are stained with Hoechst-33342 (blue). BF, bright field. Scale bar 10 µm. n.s, not significant, student T-test.

Discussion

The discovery of critical roles for certain rhomboid proteins in motility, host-cell invasion and pathogenesis of apicomplexan parasites has attracted considerable attention. However, ten years after their initial discovery, only two of the eight rhomboids of malaria parasites, ROM1 and ROM4, have been analyzed in more detail. Multiple roles have been suggested for ROM1 and ROM4: invasion of red blood cells (RBC) [22], sporozoite gliding motility [23] and the formation of the parasitophorous vacuole membrane (PVM) in infected hepatocytes [26]. In this study, we investigated expression patterns of all eight *P. berghei* rhomboids and examined the effects of rhomboid gene deletion across the entire lifecycle of the parasite in order to pinpoint additional, new role for this intramembrane protease family. In line with previously published work, our studies support the observations that ROM1 is dispensable for parasite development throughout the life cycle [25,26] and that ROM4 is essential for asexual blood stage development [22]. We identified 3 more rhomboids that are dispensable for asexual blood stage development: ROM3, ROM9 and ROM10. Mutants lacking expression of ROM9 and ROM10 can complete the entire life cycle without major developmental defects. These observations indicate functional redundancy for several rhomboids (ROM1, 9 and 10) and suggest that processing of essential substrates may be fulfilled by more than one protease. ROM4 and ROM1 are targeted to different cellular locations in the merozoite – surface and microneme [22] – making it unlikely that they process identical substrates that would allow ROM4 to compensate for ROM1 in the Δ*rom1* mutant, and clearly not vice versa.

The repeated failure to delete ROM4, ROM6, ROM7 and ROM8 genes indicate that these rhomboids play key and most likely independent roles during blood stage development that cannot be met by other proteins. Located on the merozoite surface, *P. falciparum* ROM4 is strongly implicated in the shedding of the erythrocyte binding antigen 175 (EBA175) during merozoite invasion [22]. Rodent malaria parasites lack EBA175 but express a homolog of EBA140 (BAEBL) which also belongs to the same EBL (erythrocyte-binding-like) TM protein family. Similar to EBA175, *P. falciparum* EBA140 is also an *in vitro* substrate of ROM4 [15], and in *P. yoelii* EBA140 (PY04764) is essential for RBC invasion [28]. Interestingly, in *P. berghei* the related protein, PBANKA_133270, also contains a putative cleavage site, similar to the one found in EBA140. Our successful C-terminal tagging of *P. berghei* ROM4 strengthens the notion that the failure to disrupt *rom4* is not due to inaccessibility of this specific locus to genetic modification, but is due to its key role in the enzymatic processing of surface molecules like EBA140. Combined these data suggest that ROM4 shares essential roles in both human and rodent malaria parasites

through cleavage of one or more merozoite surface proteins involved in RBC invasion, which cannot be compensated by other rhomboid or non-rhomboid proteases. ROM4 from another apicomplexan parasite, *T. gondii*, has been established as a sheddase during gliding motility and invasion [29]. In addition to ROM1 and ROM4, *P. falciparum* ROM7 and ROM8 are also expressed in merozoites [15]. It is however unlikely that these proteins process the same TM spanning proteins as ROM1 or ROM4, because they do not show the same *in vitro* substrate specificities as ROM1 or ROM4 [15]. *Plasmodium* ROM7 only has orthologs in the apicomplexan parasites, *Babesia bovis* and *Theileria annulata*, while ROM8 does not cluster with any other apicomplexan rhomboids [16].

Plasmodium ROM6 is the ortholog of *T. gondii* ROM6, which clusters with the PARL-like mitochondrial rhomboids and localizes to the single mitochondrion [16], however, a mitochondrial location in *Plasmodium* has yet to be confirmed. These ROM6 proteins share common features in their TM domains and catalytic sites, which are characteristic for PARL-type rhomboids [4], and contain predicted mitochondrial-targeting sequence [30]. Known conserved substrates of PARL-type rhomboids are dynamin-related proteins [12,14]. *Plasmodium* species express two conserved dynamins: DYN1 (PBANKA_090360) and DYN2 (PBANKA_052040). Interestingly, phylogenetic analyses show that *Plasmodium* DYN2 clusters with dynamins of other species that are mainly implicated in the division of the mitochondrial outer-membrane [31]. Attempts to disrupt the *dyn2* gene were unsuccessful (unpublished data, G.R.M. and C.J.J.; http://www.pberghei.eu/index.php?rmgm=765), suggesting its essential role in asexual stage parasites. Further research is needed to determine whether DYN2 is the substrate of ROM6 and protein localization studies with tagged proteins or antibodies may reveal whether both proteins are indeed located in the mitochondria in blood stages.

Although ROM1 is not essential for blood stage parasites, it has been reported that *P. berghei* and *P. yoelii* mutants lacking ROM1 exhibit a slight growth delay and appear less virulent in mice than wild type parasites [25,26]. In contrast, we were unable to detect either a growth or virulence-attenuation phenotype in experiments conducted with 2 independent *P. berghei* Δ*rom1* lines. The cause for these discrepancies in blood stage phenotypes between our and the *P. berghei* mutant reported by Srinivasan *et al*. [25] is unknown. In the study of Srinivasan *et al*. [25], the mutant clone examined was derived from a single transfection experiment that generated a 3' end truncation of the gene encoding ROM1, preserving a large part of the ROM1 protein. We were able to detect a stable, although truncated, transcript transcribed from the 5' end of the gene in the Δ*rom1*-p mutant; whether these are translated into stable, truncated proteins that are inserted into the membrane exerting a dominant-negative effect is unknown. Cloned

lines of wild type *P. berghei* ANKA parasites are known to differ in growth and virulence characteristics [32] and environmental factors have been shown to influence the course of infections in mice [33]; such differences between laboratories may influence the outcome of phenotypic analyses of genetically identical mutants. Therefore the reported growth and virulence phenotype may be unrelated to the disruption of *rom1*.

In contrast to normal blood stage infections of the mutants reported in this study, we found that Δ*rom1* parasites have a slight defect in liver stage development with a consistent delay of 1-day in blood stage patency following sporozoite infection. A prolonged prepatent period was also observed by Srinivasan *et al*. [25]. This finding was confirmed by a two-fold reduction in liver stage development of *P. yoelii* Δ*rom1* parasites [26]. It has been suggested that this reduction in *P. yoelii* liver development results from reduced cleavage of the PVM protein UIS4 (up-regulated in sporozoites 4) [26]. However, when we analyzed liver stage development of *P. berghei* Δ*rom1* parasites, we did not find evidence for the aborted liver stage development or parasites with unusual PVM morphology. In addition to the prolonged prepatent period, we did observe a decrease in sporozoite invasion rate in 2 out of 3 experiments. However, since there are discrepancies in Δ*rom1*-c sporozoite-hepatocyte invasion rates, we cannot conclude that a reduction in invasion is responsible for the delay in the prepatent period. Altogether, the phenotypic observations of different Δ*rom1* parasites prove that ROM1 is not essential throughout the complete life cycle in both *P. berghei* and *P. yoelii*. In addition to ROM1, our loss-of-function analyses indicate that there is large degree of functional redundancy of *Plasmodium* rhomboids. We identified two other rhomboids, ROM9 and ROM10, which are dispensable throughout the complete life cycle. Both rhomboids are exclusive to *Plasmodium* [16]. Interestingly, ROM9 carries a mitochondrial targeting sequence (MitoProtII http://ihg.gsf.de/ihg/mitoprot.html) but its predicted topology is atypical of mitochondrial PARL-like rhomboids [4]. ROM10 lacks key residues predicted to be critical to rhomboid proteolysis [4,15] and is therefore likely an inactive rhomboid. Although the expression of ROM10 was detected in multiple stages in *P. falciparum*, and our RT-PCR and Northern analyses also confirmed its expression in blood stage, the gene-deletion mutant showed no phenotypic defect throughout the entire life cycle.

In contrast to the Δ*rom1*, Δ*rom9* and Δ*rom10* parasites, mutants lacking ROM3 expression exhibit a strong and distinct phenotype. The gene encoding ROM3 is highly transcribed in gametocytes and in the *rom3*::*gfp* mutant, the GFP signal was clearly observed in female gametocytes through to the ookinete stage but was absent from developing oocysts and sporozoites. *P. berghei* mutants lacking ROM3 are capable of producing normal numbers of oocysts; however, these oocysts show a complete absence of sporozoite formation.

This is the first apicomplexan rhomboid identified to play such a vital role in sporogony. Mutant oocysts show clear signs of stalled DNA replication and a failure to form individual sporozoites, and remain highly vacuolated. This 'delayed phenotype' in mutants which lack proteins normally expressed in female gametocytes/gametes but only manifest the consequences of the loss-of-function in maturing oocysts is not unique. Examples include several members of the LCCL/lectin adhesive-like protein (CCp/LAP) family with their distinct Lgl1(LCCL)-lectin adhesive domains [34]. Deletion of these also female gametocyte expressed genes produces a phenotype in maturing oocysts comparable to the one observed in the Δ*rom3* parasites; vacuolated oocysts and absence of sporozoite formation [34–36]. CCp/LAP proteins have no TM domains and therefore are unlikely ROM3 substrates. They are localized to the crystalloid body in ookinetes which has been postulated to constitute a reservoir of proteins synthesized by the gametocyte to be used during oocyst growth and sporozoite development [37–39]. However, ultrastructure analysis of the Δ*rom3* and wild-type ookinetes revealed no distinct differences with respect to their crystalloid bodies. In addition, although we observed a punctate location of ROM3::GFP in ookinetes, we did not observe the crystalloid-type location that was shown for LAP2 and LAP3 [39]. A failure of oocysts to sporulate also occurs in the absence of three other membrane-bound proteins: glycosyl phosphatidyl inositol (GPI) anchored CSP (PBANKA_040320) [40], or TM domain containing plasmepsin VI (PBANKA_040970) [35] and PBANKA_130960 [41]. CSP is localized on the oocyst plasma membrane and on the inner surface of the oocyst capsule; when budding begins, large amounts of CSP cover the surface of sporoblasts and sporozoites [42]. Our analyses of CSP expression and processing in Δ*rom3* parasites show that although CSP expression is strongly reduced (Fig. 5B and Fig. S4), processing appears to be normal (Fig. S4). Given that CSP contains a GPI anchor it is unlikely to be processed by ROM3. As most identified natural substrates of rhomboid proteases contain only a single transmembrane domain, it is questionable if PBANKA_130960 is a substrate since it has several putative transmembrane domains (www.plasmodb.org). In Table S5 we provide a list of putative substrates of ROM3, based on the published proteome data of oocysts and sporozoite proteins (www.plasmoDB.org), which are predicted to contain a single transmembrane domain and encode a signal peptide. Whether plasmepsin VI is the substrate of ROM3 and contributes to the phenotype observed in ROM3-deficient mutants remains to be investigated. Since we observe expression of ROM3 in gametocytes and ookinetes and not in developing and mature oocysts, it is very much possible that the ROM3 substrate(s) is (are) also present and cleaved in gametocytes/ookinetes.

In this study we have examined all eight rhomboid proteases encoded by *P. berghei* and found four of them (ROM4, 6, 7 and 8) to be critical for asexual development, and one

(ROM3) essential for mosquito development. While some member of these rhomboids may govern processes common to a large number of eukaryotic species (for example, the mitochondrial PARL-like rhomboid ROM6), most of them are unique to Apicomplexa and some unique to *Plasmodium*. These specific rhomboids and their substrates offer themselves as targets for anti-parasite interventions. While the exact nature of the function of most rhomboids and their substrate range remain to be elucidated, this study helps provide a clear framework of expression, function in parasite development and the specific and redundant enzymatic activities of this important class of proteases.

Experimental procedures

Experimental animals and *P. berghei* ANKA reference lines

Female C57BL/6, BALB/c and Swiss OF1 mice (6–8 weeks) and male C57BL/6 (6–8 weeks) from Charles River were used. All animal experiments performed at the LUMC were approved by the Animal Experiments Committee of the Leiden University Medical Center (DEC 07171; DEC 10099). The Dutch Experiments on Animal Act is established under European guidelines (EU directive no. 86/609/EEC regarding the Protection of Animals used for Experimental and Other Scientific Purposes). Animals used at the Instituto de Medicina Molecular, Faculdade de Medicina, Universidade de Lisboa, were housed in the Specific Pathogen Free facilities of the Institute. All experimental procedures were carried strictly within the rules of the Portuguese official Veterinary Directorate (Direcção Geral de Veterinária), which complies with the European Guideline 86/609/EC and follows the FELASA (Federation of European Laboratory Animal Science Associations) guidelines and recommendations concerning laboratory animal welfare.

Three reference *P. berghei* ANKA parasite lines were used for generation of the gene-deletion mutants and the transgenic parasites: the 'wild type' (wt) line cl15cy1 [43] and two reporter lines, i.e. *Pb*GFP-LUC$_{con}$ (line 676m1cl1; mutant RMgm-29; www.pberghei.eu) and *Pb*GFP-Luc$_{schz}$ (line 1037cl1; mutant RMgm-32; www.pberghei.eu). Both reporter lines were generated in the cl15cy1 parent line and express the fusion protein GFP-Luciferase either under the control of the constitutive *eef1α* promoter or the schizont-specific *ama1* promoter, respectively. The *gfp-luc* expression cassette is stably integrated into the *pb230p* locus without introduction of a drug-selectable marker [44,45].

RT-PCR analyses

To investigate the transcription pattern of the different rhomboid genes, RT-PCR was performed for each gene using cDNA from i) asexual blood stages of a non-gametocyte

producer *P. berghei* ANKA parasite line (HPE) [46], ii) purified gametocytes of wild type *P. berghei* ANKA (cl15cy1) parasites and iii) salivary gland sporozoites of wild type *P. berghei* ANKA (cl15cy1). Primers were designed specific to the ORF of each gene and across introns when possible in order to distinguish amplicons from gDNA and cDNA. Details of the primers and expected sizes are shown in Table S4.

Generation of gene deletion mutants

To disrupt the *rhomboid* genes, the following replacement constructs were generated. Plasmid constructs targeting *rom1*, *3*, *4*, and *10* were constructed in the generic plasmid pL0001 (www.mr4.com) which contains the pyrimethamine resistant *Toxoplasma gondii* (*tg*) dihydrofolate reductase-thymidylate synthase (*dhfr*/*ts*) as a selectable marker (SM) under the control of *P. berghei dhfr*/*ts* promoter. Targeting regions for homologous recombination were PCR-amplified from *P. berghei* ANKA (cl15cy1) genomic DNA using primers specific for the 5'or 3' ends of each *rhomboid* gene (see Table S2 for the primer sequences) and cloned in upstream and downstream, respectively of the SM; this allows integration of the construct into the targeting regions by double cross-over homologous recombination and complete replacement of the ORF. For transfection the gene-deletion constructs were linearized with the appropriate restriction enzymes (Table S2).

Constructs targeting *rom6*, *8* and *9* were generated using a modified two step PCR method [47]. Briefly, in the first PCR reaction two fragments of 5' and 3' targeting regions (TR) were amplified from *P. berghei* ANKA (cl15cy1) genomic DNA with the primer sets shown in Table S2. The reverse primers of 5'TR and the forward primers of 3'TR have 5' extensions homologous to the h*dhfr*::y*fcu* selectable marker cassette from pL0048. In the second PCR reaction, the 5'TR and 3'TR were annealed to either side of the selectable marker cassette, and the joint fragment was amplified by the external anchor-tag primers 4661/4662, resulting in the PCR-based targeting constructs. Before transfection, the PCR-based constructs were digested with *Nru*I (as indicated in primer sequences in Table S2) to remove the 'anchor-tag' and with *Dpn*I that digests any residual uncut pL0048 plasmid.

Transfection and selection of transformed parasites with pyrimethamine was performed using standard technology for the genetic modification of *P. berghei* [43]. All information on the generation of gene-deletion mutants (as well as unsuccessful disruption attempts), such as DNA constructs and primers, has been submitted to the RMgmDB database of genetically modified rodent malaria parasites (www.pberghei.eu).

Clonal parasite lines were obtained from all gene-deletion mutants by the method of limiting dilution. Correct integration of DNA constructs and disruption of the genes was

verified by diagnostic PCR analyses (see Table S3 for primers used) and Southern analyses of chromosomes separated by pulsed-field gel electrophoresis hybridized with probes specific for the selectable maker (see Table S3 for primers used) [43].

Generation and analyses of parasites expressing ROM3::GFP and ROM4::mCherry

To tag ROM3 C-terminally with GFP, 1.6 kb upstream of the stop codon of *rom3* containing the entire ORF were PCR-amplified from wild-type *P. berghei* ANKA genomic DNA, TOPO-cloned and sequence analyzed (see Table S2 for the primers). The fragment was released from pCR2.1-TOPO (Invitrogen) through digestion with *EcoR*V and *BamH*I and ligated into the generic GFP-tagging plasmid pL1200 [48], resulting in construct pL1079 containing the pyrimethamine resistant *tgdhfr*/*ts* as a selectable marker. To tag ROM4 with mCherry, the complete ORF of *rom4* (except the stop codon) was PCR-amplified from wild type *P. berghei* ANKA genomic DNA (see Table S2 for the primers used). This ORF was digested with *Spe*I and *Bgl*II, and ligated into *Spe*I/*BamH*I digested vector pL1646 (containing a C-terminal mCherry tag and the *tgdhfr*/*ts* selectable marker cassette), resulting in construct pL1920. Before transfection, pL1709 was linearized with *Spe*I, and pL1920 was linearized with *BamH*I. Transfection, selection and cloning of transgenic parasites with pyrimethamine was carried out as described above, generating the following transgenic lines, *rom3::gfp* (line 654cl1) and *rom4::mCherry* (line 2143cl1) that express endogenous C-terminally tagged ROM3 and ROM4, respectively. The live GFP or mCherry signals of parasites of the transgenic mutants were examined by fluorescence microscopy (Leica DM-IRBE Flu) after staining with Hoechst-33342 (2 µmol/L, Sigma, NL) for 15 min at room temperature. The fluorescence intensity was measured using ImageJ software.

Analysis of transcription of rhomboid genes in blood stages of wild type and gene-deletion parasites

Transcript levels were analyzed by standard Northern blot analyses. Total RNA was isolated from mixed blood stages or different stages of wild type *P. berghei* ANKA (cl15cy1), non-gametocyte producer line (HPE) and the different gene-deletion mutant lines. Northern blots were hybridised with probes specific for each rhomboid ORF, which had been PCR-amplified from wild-type *P. berghei* ANKA genomic DNA (primers shown in Table S3). As a loading control, Northern blots were hybridized with the oligonucleotide probe L644R that recognizes the large subunit ribosomal RNA [49].

In vivo multiplication rate of asexual blood stages

The multiplication rate of asexual blood stages in mice is determined during the cloning procedure of each gene-deletion mutant [45] and is calculated as follows: the percentage of infected erythrocytes in Swiss OF1 mice injected with a single parasite is quantified at day 8 to 11 on Giemsa-stained blood films. The mean asexual multiplication rate per 24 hour is then calculated assuming a total of 1.2×10^{10} erythrocytes per mouse (2mL of blood). The percentage of infected erythrocytes in mice infected with reference lines of the *P. berghei* ANKA strain consistently ranges between 0.5–2% at day 8 after infection, resulting in a mean multiplication rate of 10 per 24h [45,50].

Course of parasitemia, virulence and experimental cerebral malaria in mice infected with Δ*rom1* parasites

The course of parasitemia was determined in BALB/c mice. Groups of 6 mice were intraperitoneally (i.p) infected with 10^4 Δ*rom1*-c parasites or equal numbers of the parental reporter line *Pb*GFP-LUC_{con}. The course of parasitemia was determined in a luciferase assay (IVDL-assay) [51]; *in vivo* parasite growth in mice is quantified by measuring the luciferase activity of GFP-Luciferase expressing parasites in tail blood. The IVDL-assay generates growth-curves that are identical to those obtained by manual counting of parasites in Giemsa-stained smears. In brief, 10 µL tail blood was collected daily from all mice using heparinized capillaries. Samples were stored at -80 °C in Eppendorf tubes till further processing for the luciferase assay. Luciferase activity (luminescence) in the samples was measured as described [51,52].

The capacity of Δ*rom1* to induce features of experimental cerebral malaria (ECM) was analyzed in C57BL/6 mice. Groups of 6 mice were infected with 10^5 *P. berghei* ANKA (cl15cy1), Δ*rom1*-p or Δ*rom1*-c parasites. Onset of ECM in *P. berghei* infection was determined by measurement of a drop in body temperature below 34°C [45]. The body temperature of infected mice was measured twice a day from day 5 to day 8 after infection using a laboratory thermometer (model BAT-12, Physitemp Instruments Inc., Clifton, NJ) with a rectal probe (RET-2) for mice. When infected mice showed a drop in temperature (below 34°C) the mice were sacrificed.

Gametocyte and ookinete production

Gametocyte production is defined as the percentage of ring forms developing into mature gametocytes during synchronized infections [53]. Ookinete production was determined in standard *in vitro* fertilization and ookinete maturation assays and is defined as the

percentage of female gametes that develop into mature ookinetes under standardized *in vitro* culture conditions [54]. Female gamete and mature ookinete numbers were determined in Giemsa-stained blood smears made 16–18 h post activation.

Electron microscopy

Ookinetes were cultured *in vitro* as previously described [54]; briefly, gametocytes for these assays were obtained from infected mice that had been pre-treated with phenylhydrazine and treated with the antimalarial drug sulfadiazine (dissolved in the drinking water at a concentration of 30 mg/L) to obtain highly pure gametocyte populations [55]. Ookinetes from these cultures were purified using a Nycodenz density gradient centrifugation. The purified ookinetes were diluted in RPMI medium (without serum) and fixed by resuspending them in an equal amount of 3% glutaraldehyde (Electron Microscopy Sciences, Hatfield, PA) in 0.2 M sodium cacodylate pH 7.4 (1h at RT), washed twice with cacodylate buffer (spinning for 2min at 425*g*), post-fixed with 1% osmium tetroxide (Electron Microscopy Sciences, Hatfield, PA) in cacodylate buffer (1h at RT), and washed again with cacodylate buffer. Subsequently, the samples were stained with an aqueous solution of 1% uranyl acetate for 40 min at RT, washed twice with demineralized water, re-suspended in 3% agar (Difco Laboratories, Detroit, Michigan; in demineralized water at 60°C), centrifuged (for 2min at 425*g*) and stored at 4°C until the agar became solid. The samples were dehydrated in series of washes 70% (overnight), 80% (10 min), 90% (10 min) and 100% ethanol (1h, refreshing 2 times) , infiltrated with a 1:1 mixture of epon LX 112/propylene oxide (1h) and pure epon (3h), followed by embedding in epon and polymerization for 48h at 60°C. The samples were cut using a Leica UC6 ultramicrotome at RT into 100nM sections with a Diatome ultra 45°diamond knife (Diatome, Switzerland) at a cutting speed of 1 mm/s. The sections were attached to slot copper grids (Stork Veco BV, Eerbeek, The Netherlands), covered with 1% formvar film and a 7nm carbon layer; no post-staining was applied prior to data collection. Imaging was performed in a Tecnai 12 Twin transmission electron microscope (FEI Company). Transmission electron microscope was operated at an acceleration voltage of 80 kV, and binned images (2kx2k) were acquired with a FEI Eagle CCD camera (FEI Company).

Oocyst and sporozoite production in *Anopheles stephensi* mosquitoes

For mosquito transmission experiments female *A. stephensi* mosquitoes were fed on mice infected with wild-type parasites or mutants. Oocyst development, oocyst production and sporozoite production was monitored in infected mosquitoes as described [56]. Oocyst and sporozoites numbers were counted in infected mosquitoes at 11–14 days

and 19–22 days after infection, respectively. Salivary gland sporozoites were isolated and counted as described [57].

For Western Blot analysis of CSP expression in oocysts or sporozoites, we isolated oocysts containing midguts from infected mosquitoes, or 100,000 midgut sporozoites, and proteins were separated on 8% polyacrylamide gels and transferred to nitrocellulose membranes by electroblotting. CSP expression was detected by incubation of membranes with monoclonal anti-CSP antibody [58] followed by incubation with horseradish-peroxidase-conjugated anti-mouse antibody (Sigma). Immunostained protein complexes were visualized by enhanced chemiluminescence (Amersham). For the immunofluorescence assays (IFA), midguts of infected mosquitoes were isolated in RPMI-Medium and immobilised with 2% formaldehyde, 0.2% glutaraldehyde, 2mM magnesium chloride, 0.02% Triton-X 100 in phosphate buffered saline (PBS). Subsequently midguts were permeabilized, using 2% Saponin in PBS and oocysts stained with monoclonal anti-CSP antibody and monoclonal Alexa-Fluor® 488 goat anti-mouse antibody. DNA was stained with Hoechst-33342.

Sporozoite infectivity and liver stage development

Sporozoites were collected at day 19–25 after infection by hand-dissection of the salivary glands as described [57]. Gliding motility of sporozoites was determined in assays that were performed on anti-*P. berghei* CSP antibody (3D11, monoclonal mouse antibody 25 µg/ml, 100 µl/well) pre-coated 10 well cell-line diagnostic microscope slides (7mm, Thermo Scientific) to which 1×10^4 sporozoites were added [59]. After 30 min of incubation at 37°C sporozoites were fixed with 4% paraformaldehyde and after washing with PBS, the sporozoites and the trails ('gliding circles') were stained with anti-CSP-antiserum [60] and anti-rabbit IgG- secondary antibody (Alexa Fluor® 488 Goat Anti-rabbit IgG; Molecular Probes®, Invitrogen). Slides were mounted with Vectorshield (Vector Laboratories Inc) and 'gliding circles' were analyzed using a Leica DMR fluorescence microscope at 1000× magnification.

Huh-7 cells, a human hepatoma cell line, were used in *in vitro* analysis of sporozoite infectivity. Huh-7 cells were cultured in 'complete' RPMI 1640 medium supplemented with 10% (v/v) fetal bovine serum (FBS), 1% (v/v) penicillin-streptomycin, 1% (v/v) GultaMAX (Invitrogen), and maintained at 37°C with 5% CO_2. Sporozoite hepatocyte traversal was determined in assays as described previously [61]. Briefly, Huh-7 cells were suspended in 1mL of 'complete' medium and were seeded in 24 well plates (10^5 cells/mL). After the Huh7 monolayers were >80% confluent, 10^5 sporozoites were added with the addition of FITC- or Alexa-647-labeled dextran (Invitrogen, NL) for 2 h. No sporozoites were added

to the negative control wells. *In vitro* invasion rates of mutants lacking expression of rhomboids and wild type parasites were determined by the ratio between the number of sporozoites inside the cells and the total number of sporozoites (both inside and outside of cells). Huh-7 cells (5×10^4 cells per well) were seeded into coverslips in 24-well plates and on the following day, cells were infected with 5×10^4 sporozoites. Three hours after infection, cells were fixed with 4% paraformaldehyde in PBS for 20 min. For the double staining, cells were incubated for 30 min in blocking buffer (10% FBS in PBS) followed by 1 hour incubation with anti-CSP serum against *P. berghei* circumsporozoite protein (CSP) protein [60] diluted 1:500 in the same buffer. Cells were then washed with PBS and incubated for 45 min with a secondary antibody (anti-rabbit Alexa Fluor® 568) diluted 1:500 in blocking buffer. This procedure only stained the parasites outside the cells. After washing with PBS, cells were fixed with 4% paraformaldehyde in PBS for 30 min, then incubated in for 30 min in permeabilization buffer (1% Triton X-100 in PBS) followed by 1 h incubation with anti-CSP serum diluted 1:500 in the same buffer. Cells were then washed with PBS and incubated for 45 min with a secondary antibody (anti-rabbit Alexa Fluor® 488) diluted 1:500 in blocking buffer. This second staining allows visualization of all the parasites, whether inside or outside the cells. Nuclei were stained with Hoechst-33342. The parasites in both green and red channels were analyzed using a DM-IRBE Flu Leica fluorescence microscope.

For analysis of *in vitro* EEF (exo-erythrocytic form) development, 5×10^4 sporozoites were added to a monolayer of Huh7 cells on coverslips in 24 well plates in 'complete' RPMI 1640 (see above). At different time points after infection, cells were fixed with 4% paraformaldehyde, permeabilized with 0.5% Triton-X-100 in PBS, blocked with 10% FBS in PBS, and subsequently stained with primary and secondary antibodies for 2h and 1h, respectively. Primary antibodies used were anti-PbEXP1 (raised in chicken [62]) and anti-UIS4 (raised in rabbit [63], detecting the PVM-resident proteins; anti-PbHSP70 (raised in mouse [59]), detecting the cytoplasmic heat shock protein 70 (PBANKA_081890); and anti-MSP1 (mouse; MRA-78 from MR4; www.MR4.org) detecting MSP1 of *P. yoelii* and *P. berghei*. Anti-mouse, -chicken and -rabbit secondary antibodies, conjugated to Alexa Fluor® 488 and 594, were used for visualization (Invitrogen). Nuclei were stained with Hoechst-33342. Cells were mounted in Vectashield (Vector Laboratories Inc) and examined using a DM-IRBE Flu Leica fluorescence microscope.

In addition, Intracellular parasite development was determined by measuring the area of the EEFs inside fixed Huh-7 hepatoma cells. Huh-7 cells (5×10^4 cells per well) were seeded into coverslips in 24-well plates and, the following day, cells were infected with 4×10^4 sporozoites. Forty-eight hours after infection, cells were fixed with 4% paraformaldehyde

in PBS for 20 min. Cells were stained by incubation for 30 min in blocking/permeabilization buffer (0.5% Triton X-100, 1% BSA in PBS) followed by 1 h incubation with monoclonal antibody 2E6 against *P. berghei* HSP70 diluted 1:500 in the same buffer. Cells were then washed with 0.5% Triton X-100 in PBS and incubated for 45 min with a secondary antibody (anti-mouse Alexa488) diluted 1:400 in blocking/permeabilization buffer. Nuclei were stained with DAPI. Images were acquired with a Zeiss Axiovert 200M widefield fluorescence microscope and processed using ImageJ.

Hepatocyte infection was determined by measuring the luminescence intensity in Huh-7 cells infected with either the firefly luciferase-expressing Δ*rom9* and the corresponding control line PbGFP-Luc_{schz}. Huh-7 cells infection and culture conditions were as described above. At 57 h after infection, 50 µL of D-Luciferin (Firefly Luciferase Assay Kit, Biotium) were added to 30 µL of lysed samples in white 96-well plates. Luminescence intensity of the samples was measured using a microplate reader (Tecan Infinite M200). The viability of Huh-7 cells was assessed by the AlamarBlue assay (Invitrogen, United Kingdom) according to the manufacturer's protocol.

To determine parasite loads by qRT-PCR, sporozoites (5×10^4) were added to a monolayer of Huh7 cells (seeded the day before with 10^5 cells) in 24 well plates in 'complete' DMEM (see above). At different time-points after adding the sporozoites, culture medium was removed, cells washed once with PBS, and cells were resuspended in 200 µL of RLT buffer (Quiagen's MicroRNeasy kit). RNA from these samples was extracted following the manufacturer's instructions. The transcriptor first-strand cDNA synthesis kit (Roche) was used according to the manufacturer's recommendations to make single-stranded cDNA. Real time PCR analysis of *P. berghei* 18S rRNA and human β-actin was performed as described [64].

Flow cytometry analysis was used to determine the parasite load of Δ*rom9* in Huh-7 cell (57 h p.i) compared the wild type control (PbGFP-Luc_{schz}). The infection and culture condition was as described above. 57 h after infection, samples for were washed with PBS, incubated with trypsin for 5 min at 37°C and collected in 400 µL of 10% v/v FBS in PBS. Cells were then centrifuged at 0.1 g for 5 min, resuspended in 300 µL of 2% v/v FBS in PBS. All samples were analyzed on a LSR Fortessa cytometer with the appropriate settings for the fluorophores used. Data acquisition and analysis were carried out using the BD FACSDiva (BD Biosciences) and FlowJo (v6.4.7, FlowJo) software packages respectively.

To determine *in vivo* infectivity of sporozoites, Swiss OF1 mice were infected with 1×10^4 salivary gland sporozoites by intravenous injection, as previously described [56]. Blood stage infections were monitored by analysis of Giemsa-stained thin smears of tail blood collected on day 4–8 after inoculation of sporozoites. The prepatent period (measured in

days post sporozoite infection) is defined as the day when a blood stage infection with a parasitemia of 0.5–2% is observed. In addition we determined parasite loads in livers of infected mice by *in vivo* imaging as described [64]. In addition, a group of 10 male C57BL/6 mice were inoculated by i.v. injection of 1×10^4 freshly isolated sporozoites of Δ*rom9* or its wild type control PbGFP-Luc_{schz}. Luciferase activity in the livers of the animals was visualized 44 hours after infection using an *in vivo* Imaging System (IVIS Lumina), following i.p injection of D-luciferin dissolved in PBS (100 mg/kg). Animals were kept under anesthesia during the measurements, which were performed within 3 to 5 min after the injection of D-luciferin. Bioluminescence imaging was acquired with a 10 cm field of view, medium binning factor and an exposure time of 180 seconds. Quantitative analysis of bioluminescence was performed by measuring the luminescence signal intensity using the ROI settings of the Living Image® 3.0 software. ROI measurements are expressed in total flux of photons. qRT-PCR is also used to determine the *in vivo* parasite load in liver. After measuring luminescence, livers from 5 mice were collected, homogenized in 4 mL denaturing solution (4 M guanidine thiocyanate; 25 mM sodium citrate pH 7, 0.5 % sarcosyl and 0.7 % β-Mercaptoethanol in DEPC-treated water) and total RNA was extracted using the RNeasy Mini kit (Qiagen). cDNA was obtained by reverse transcription (First-strand cDNA synthesis kit, Roche) and qRT-PCR using the SybrGreen method (DyNAmoTM HS SYBR® Green qPCR Kit, Finnzymes) was performed with primers specific for *P. berghei* 18S rRNA for quantification of parasite load in the liver of each mouse. Relative amounts of *P. berghei* mRNA were calculated against the Hypoxanthine Guanine Phosphoribosyl Transferase (HPRT) housekeeping gene [64].

Acknowledgements

We thank Inês S. Albuquerque and Hans Kroeze for technical assistance. Jing-wen Lin is supported by the China Scholarship Council-Leiden University Joint Program and Chris J Janse, Andy Waters, Kai Matuschewski by a grant of the European Community's Seventh Framework Programme (FP7/2007–2013) under grant agreement no. 242095. Gunnar Mair is supported by FCT (PTDC/BIA-BCM/ 105610/2008, PTDC/SAU-GMG/104392/2008 and PTDC/SAU-MIC/122082/2010), Patrícia Meireles by FCT grant SFRH/BD/71098/2010 and Miguel Prudêncio by FCT project grant PTDC/SAUMIC/117060/2010.

References

1. Freeman M (2004) Proteolysis within the membrane: rhomboids revealed. Nat Rev Mol Cell Biol 5: 188-197.
2. Urban S, Lee JR, Freeman M (2001) Drosophila rhomboid-1 defines a family of putative intramembrane serine proteases. Cell 107: 173-182.
3. Koonin EV, Makarova KS, Rogozin IB, Davidovic L, Letellier MC, Pellegrini L (2003) The rhomboids: a nearly ubiquitous family of intramembrane serine proteases that probably evolved by multiple ancient horizontal gene transfers. Genome Biol 4: R19.
4. Lemberg MK, Freeman M (2007) Functional and evolutionary implications of enhanced genomic analysis of rhomboid intramembrane proteases. Genome Res 17: 1634-1646.
5. Wang Y, Zhang Y, Ha Y (2006) Crystal structure of a rhomboid family intramembrane protease. Nature 444: 179-180.
6. Wu Z, Yan N, Feng L, Oberstein A, Yan H, Baker RP, *et al* (2006) Structural analysis of a rhomboid family intramembrane protease reveals a gating mechanism for substrate entry. Nat Struct Mol Biol 13: 1084-1091.
7. Ben-Shem A, Fass D, Bibi E (2007) Structural basis for intramembrane proteolysis by rhomboid serine proteases. Proc Natl Acad Sci U S A 104: 462-466.
8. Urban S, Schlieper D, Freeman M (2002) Conservation of intramembrane proteolytic activity and substrate specificity in prokaryotic and eukaryotic rhomboids. Curr Biol 12: 1507-1512.
9. Urban S, Lee JR, Freeman M (2002) A family of Rhomboid intramembrane proteases activates all Drosophila membrane-tethered EGF ligands. EMBO J 21: 4277-4286.
10. Sundaram MV (2004) Vulval development: the battle between Ras and Notch. Curr Biol 14: R311-R313.
11. Stevenson LG, Strisovsky K, Clemmer KM, Bhatt S, Freeman M, Rather PN (2007) Rhomboid protease AarA mediates quorum-sensing in Providencia stuartii by activating TatA of the twin-arginine translocase. Proc Natl Acad Sci U S A 104: 1003-1008.
12. McQuibban GA, Saurya S, Freeman M (2003) Mitochondrial membrane remodelling regulated by a conserved rhomboid protease. Nature 423: 537-541.
13. Cipolat S, Rudka T, Hartmann D, Costa V, Serneels L,*et al* (2006) Mitochondrial rhomboid PARL regulates cytochrome c release during apoptosis via OPA1-dependent cristae remodeling. Cell 126: 163-175.
14. Dowse TJ, Soldati D (2005) Rhomboid-like proteins in Apicomplexa: phylogeny and nomenclature. Trends Parasitol 21: 254-258.
15. Baker RP, Wijetilaka R, Urban S (2006) Two *Plasmodium* rhomboid proteases preferentially cleave different adhesins implicated in all invasive stages of malaria. PLoS Pathog 2: e113.
16. Santos M, Graindorge A, Soldati-Favre D (2011) New insights into parasite rhomboid proteases. Mol Biochem Parasitol . S0166-6851(11)00285-4

17. Freeman M (2009) Rhomboids: 7 years of a new protease family. Semin Cell Dev Biol 20: 231-239. S1084-9521(08)00115-8

18. Buguliskis JS, Brossier F, Shuman J, Sibley LD (2010) Rhomboid 4 (ROM4) affects the processing of surface adhesins and facilitates host cell invasion by *Toxoplasma gondii*. PLoS Pathog 6: e1000858.

19. Santos JM, Ferguson DJ, Blackman MJ, Soldati-Favre D (2011) Intramembrane cleavage of AMA1 triggers *Toxoplasma* to switch from an invasive to a replicative mode. Science 331: 473-477. science.1199284

20. Brossier F, Jewett TJ, Sibley LD, Urban S (2005) A spatially localized rhomboid protease cleaves cell surface adhesins essential for invasion by *Toxoplasma*. Proc Natl Acad Sci U S A 102: 4146-4151.

21. Brossier F, Starnes GL, Beatty WL, Sibley LD (2008) Microneme rhomboid protease TgROM1 is required for efficient intracellular growth of *Toxoplasma gondii*. Eukaryot Cell 7: 664-674.

22. O'Donnell RA, Hackett F, Howell SA, Treeck M, Struck N, Krnajski Z, *et al* (2006) Intramembrane proteolysis mediates shedding of a key adhesin during erythrocyte invasion by the malaria parasite. J Cell Biol 174: 1023-1033.

23. Ejigiri I, Ragheb DRT, Pino P, Coppi A, Bennett BL, *et al* (2012) Shedding of TRAP by a Rhomboid Protease from the Malaria Sporozoite Surface Is Essential for Gliding Motility and Sporozoite Infectivity. PLoS Pathog 8: e1002725.

24. Olivieri A, Collins CR, Hackett F, Withers-Martinez C, Marshall J, *et al* (2011) Juxtamembrane shedding of *Plasmodium falciparum* AMA1 is sequence independent and essential, and helps evade invasion-inhibitory antibodies. PLoS Pathog 7: e1002448.

25. Srinivasan P, Coppens I, Jacobs-Lorena M (2009) Distinct roles of *Plasmodium* rhomboid 1 in parasite development and malaria pathogenesis. PLoS Pathog 5: e1000262.

26. Vera IM, Beatty WL, Sinnis P, Kim K (2011) *Plasmodium* protease ROM1 is important for proper formation of the parasitophorous vacuole. PLoS Pathog 7: e1002197.

27. Khan SM, Franke-Fayard B, Mair GR, Lasonder E, Janse CJ, *et al* (2005) Proteome analysis of separated male and female gametocytes reveals novel sex-specific *Plasmodium* biology. Cell 121: 675-687.

28. Otsuki H, Kaneko O, Thongkukiatkul A, Tachibana M, Iriko H, *et al* (2009) Single amino acid substitution in *Plasmodium yoelii* erythrocyte ligand determines its localization and controls parasite virulence. Proc Natl Acad Sci U S A 106: 7167-7172. 0811313106

29. Parussini F, Tang Q, Moin SM, Mital J, Urban S, Ward GE (2012) Intramembrane proteolysis of *Toxoplasma* apical membrane antigen 1 facilitates host-cell invasion but is dispensable for replication. Proc Natl Acad Sci U S A 109: 7463-7468.

30. Verma R, Varshney GC, Raghava GP (2010) Prediction of mitochondrial proteins of malaria parasite using split amino acid composition and PSSM profile. Amino Acids 39: 101-110.

31. Charneau S, Bastos IM, Mouray E, Ribeiro BM, Santana JM, *et al* (2007) Characterization of PfDYN2, a dynamin-like protein of *Plasmodium falciparum* expressed in schizonts. Microbes Infect 9: 797-805.

32. Amani V, Boubou MI, Pied S, Marussig M, Walliker D, *et al* (1998) Cloned lines of *Plasmodium berghei* ANKA differ in their abilities to induce experimental cerebral malaria. Infect Immun 66: 4093-4099.

33. Levander OA, Fontela R, Morris VC, Ager AL, Jr. (1995) Protection against murine cerebral malaria by dietary-induced oxidative stress. J Parasitol 81: 99-103.

34. Raine JD, Ecker A, Mendoza J, Tewari R, Stanway RR, Sinden RE (2007) Female inheritance of malarial lap genes is essential for mosquito transmission. PLoS Pathog 3: e30.

35. Ecker A, Bushell ES, Tewari R, Sinden RE (2008) Reverse genetics screen identifies six proteins important for malaria development in the mosquito. Mol Microbiol 70: 209-220.

36. Lavazec C, Moreira CK, Mair GR, Waters AP, Janse CJ, Templeton TJ (2009) Analysis of mutant *Plasmodium berghei* parasites lacking expression of multiple PbCCp genes. Mol Biochem Parasitol 163: 1-7.

37. Garnham PC, Bird RG, Baker JR (1962) Electron microscope studies of motile stages of malaria parasites. III. The ookinetes of Haemamoeba and *Plasmodium*. Trans R Soc Trop Med Hyg 56: 116-120.

38. Garnham PC, Bird RG, Baker JR, Desser SS, el-Nahal HM (1969) Electron microscope studies on motile stages of malaria parasites. VI. The ookinete of *Plasmodium berghei yoelii* and its transformation into the early oocyst. Trans R Soc Trop Med Hyg 63: 187-194.

39. Saeed S, Carter V, Tremp AZ, Dessens JT (2010) *Plasmodium berghei* crystalloids contain multiple LCCL proteins. Mol Biochem Parasitol 170: 49-53.

40. Menard R, Sultan AA, Cortes C, Altszuler R, van Dijk MR, *et al* (1997) Circumsporozoite protein is required for development of malaria sporozoites in mosquitoes. Nature 385: 336-340.

41. Lasonder E, Janse CJ, van Gemert GJ, Mair GR, Vermunt AM, *et al* (2008) Proteomic profiling of *Plasmodium* sporozoite maturation identifies new proteins essential for parasite development and infectivity. PLoS Pathog 4: e1000195.

42. Thathy V, Fujioka H, Gantt S, Nussenzweig R, Nussenzweig V, Menard R (2002) Levels of circumsporozoite protein in the *Plasmodium* oocyst determine sporozoite morphology. EMBO J 21: 1586-1596.

43. Janse CJ, Ramesar J, Waters AP (2006) High-efficiency transfection and drug selection of genetically transformed blood stages of the rodent malaria parasite *Plasmodium berghei*. Nat Protoc 1: 346-356.

44. Janse CJ, Franke-Fayard B, Mair GR, Ramesar J, Thiel C, *et al*(2006) High efficiency transfection of *Plasmodium berghei* facilitates novel selection procedures. Mol Biochem Parasitol 145: 60-70.

45. Spaccapelo R, Janse CJ, Caterbi S, Franke-Fayard B, Bonilla JA, Syphard LM, *et al* (2010) Plasmepsin 4-deficient *Plasmodium berghei* are virulence attenuated and induce protective immunity against experimental malaria. Am J Pathol 176: 205-217. S

46. Janse CJ, Boorsma EG, Ramesar J, van VP, van der MR, *et al* (1989) *Plasmodium berghei*: gametocyte production, DNA content, and chromosome-size polymorphisms during asexual multiplication *in vivo*. Exp Parasitol 68: 274-282.

47. Lin JW, Annoura T, Sajid M, Chevalley-Maurel S, Ramesar J, *et al* (2011) A Novel 'Gene Insertion/ Marker Out' (GIMO) Method for Transgene Expression and Gene Complementation in Rodent Malaria Parasites. PLoS One 6: e29289.

48. Mair GR, Lasonder E, Garver LS, Franke-Fayard BM, Carret CK, *et al*(2010) Universal features of post-transcriptional gene regulation are critical for *Plasmodium* zygote development. PLoS Pathog 6: e1000767.

49. van Spaendonk RM, Ramesar J, van WA, Eling W, Beetsma AL, *et al* (2001) Functional equivalence of structurally distinct ribosomes in the malaria parasite, *Plasmodium berghei*. J Biol Chem 276: 22638-22647.

50. Janse CJ, Haghparast A, Speranca MA, Ramesar J, Kroeze H, *et al* (2003) Malaria parasites lacking eef1a have a normal S/M phase yet grow more slowly due to a longer G1 phase. Mol Microbiol 50: 1539-1551.

51. Franke-Fayard B, Djokovic D, Dooren MW, Ramesar J, Waters AP, *et al* (2008) Simple and sensitive antimalarial drug screening *in vitro* and *in vivo* using transgenic luciferase expressing *Plasmodium berghei* parasites. Int J Parasitol 38: 1651-1662.

52. Lin JW, Sajid M, Ramesar J, Khan SM, Janse CJ, Franke-Fayard B (2013) Screening Inhibitors of *P. berghei* Blood Stages Using Bioluminescent Reporter Parasites. Methods Mol Biol 923: 507-522.

53. Janse CJ, Waters AP (1995) *Plasmodium berghei*: the application of cultivation and purification techniques to molecular studies of malaria parasites. Parasitol Today 11: 138-143.

54. van Dijk MR, Janse CJ, Thompson J, Waters AP, Braks JA, *et al* (2001) A central role for P48/45 in malaria parasite male gamete fertility. Cell 104: 153-164.

55. Beetsma AL, van de Wiel TJ, Sauerwein RW, Eling WM (1998) *Plasmodium berghei* ANKA: purification of large numbers of infectious gametocytes. Exp Parasitol 88: 69-72.

56. Sinden R.E. (1997) Infection of mosquitoes with rodent malaria. In: Crampton J.M., Beard C.B., Louis C., editors. Molecular biology of insect disease vectors: a method manual. London, United Kingdom: Chapman and Hall. pp. 67-91.

57. Annoura T, Ploemen IH, van Schaijk BC, Sajid M, Vos MW, *et al* (2012) Assessing the adequacy of attenuation of genetically modified malaria parasite vaccine candidates. Vaccine 30: 2662-2670.

58. Potocnjak P, Yoshida N, Nussenzweig RS, Nussenzweig V (1980) Monovalent fragments (Fab) of monoclonal antibodies to a sporozoite surface antigen (Pb44) protect mice against malarial infection. J Exp Med 151: 1504-1513.

59. van Dijk MR, Douradinha B, Franke-Fayard B, Heussler V, van Dooren MW, *et al* (2005) Genetically attenuated, P36p-deficient malarial sporozoites induce protective immunity and apoptosis of infected liver cells. Proceedings of the National Academy of Sciences of the United States of America 102: 12194-12199.

60. Yoshida N, Nussenzweig RS, Potocnjak P, Nussenzweig V, Aikawa M (1980) Hybridoma produces protective antibodies directed against the sporozoite stage of malaria parasite. Science 207: 71-73.

61. Mota MM, Pradel G, Vanderberg JP, Hafalla JCR, Frevert U, Nussenzweig RS, Nussenzweig V, Rodriguez A (2001) Migration of *Plasmodium* sporozoites through cells before infection. Science 291: 141-144.

62. Sturm A, Amino R, van de SC, Regen T, Retzlaff S, Rennenberg A, *et al* (2006) Manipulation of host hepatocytes by the malaria parasite for delivery into liver sinusoids. Science 313: 1287-1290.

63. Mueller AK, Camargo N, Kaiser K, Andorfer C, Frevert U, *et al* (2005) *Plasmodium* liver stage developmental arrest by depletion of a protein at the parasite-host interface. Proc Natl Acad Sci U S A 102: 3022-3027. 0408442102

64. Ploemen IH, Prudencio M, Douradinha BG, Ramesar J, Fonager J, *et al* (2009) Visualisation and quantitative analysis of the rodent malaria liver stage by real time imaging. PLoS ONE 4: e7881.

Supplementary Material

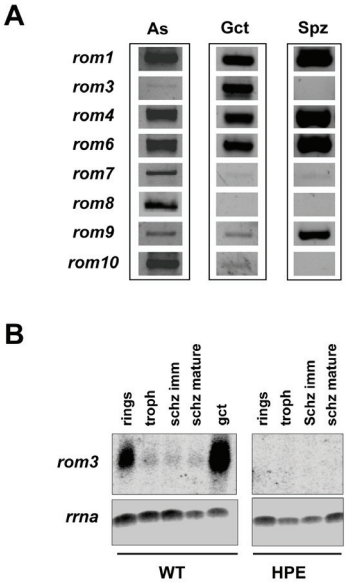

Figure S1. RT-PCR and Northern blot analyses of rhomboid transcription

A. Transcription patterns of different rhomboids as determined by RT-PCR using cDNA from i) asexual blood stages of a non-gametocyte producer *P. berghei* ANKA parasite line (HPE), ii) purified gametocytes of wild type *P. berghei* ANKA (cl15cy1) parasites and iii) salivary gland sporozoites of wild type *P. berghei* ANKA (cl15cy1). Details of the primers and expected sizes of the amplified products are shown in Table S4.

B. Northern analysis of *rom3* transcription. Total RNA was isolated from synchronized blood stages and purified gametocytes (gct) of wild type (WT) *P. berghei* ANKA (cl15cy1) and from blood stages of the non-gametocyte producer *P. berghei* ANKA parasite line (HPE). Transcripts were only detected in WT parasites with high level of expression in gametocytes. Signals in rings are the result of contamination with gametocytes in synchronized infections (Janse and Waters, 1995). Hybridization was performed using a PCR probe recognizing the *rom3* gene (primers 1812/1813). As a loading control, hybridization was performed with probe L644R that recognizes the large subunit ribosomal RNA (see Table S4 for primer sequences). Rings (5 h post invasion, hpi); troph (trphozoites, 16hpi); schz imm (immature schizonts; 20hpi); schz mature (mature schizonts 24hpi); gct (gametocytes).

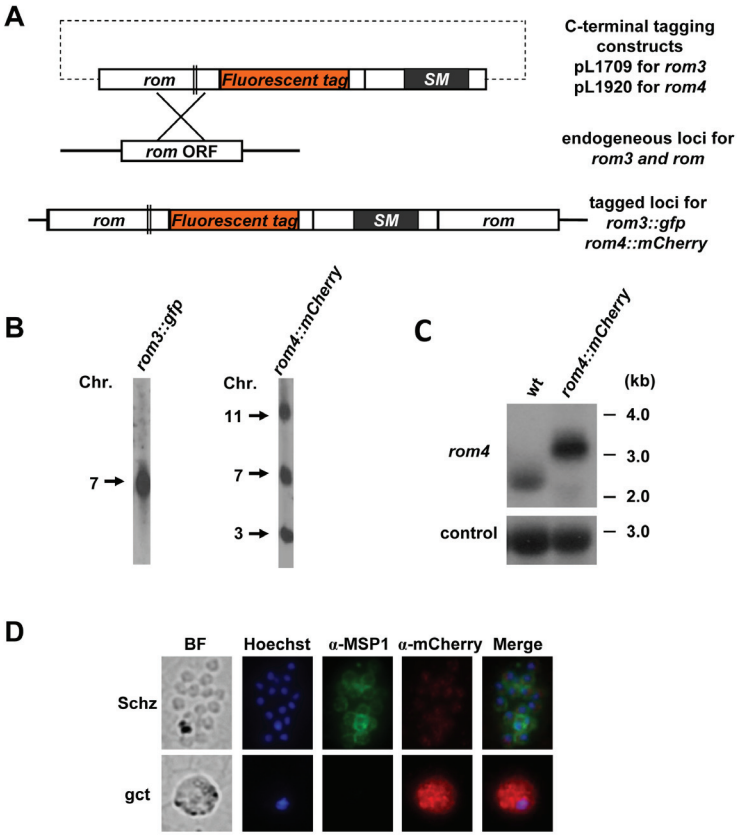

Figure S2. Generation of transgenic lines expressing C-terminally fluorescent-tagged ROM3 and ROM4.

A. Schematic representation of the tagging constructs pL1709 and pL1920 targeting *rom3* and *rom4* respectively by single cross-over homologous recombination, and the locus before and after tagging. The tagging constructs contain C-terminal fluorescent tag (orange boxes) and the *tgdhfr/ts* drug selectable marker cassette (SM; black boxes). The double lines indicate the enzyme site used for construct linearization.

B. Southern analyses of pulsed field gel-separated chromosomes confirm correct integration of the two tagging constructs. Chromosomes of *rom3::gfp* line (left) were hybridized using a *tgdhfr/ts* probe that recognizes the construct integrated into *rom3* locus on chromosome 7. Chromosomes of *rom4::mCherry* line were hybridized with a 3'UTR *pbdhfr* probe recognizing the tagging construct integrated into the *rom4* locus on chromosome 11, the endogenous *dhfr/ts* gene on chromosome 7 and the GFP-luciferase reporter cassette introduced in chromosome 3 (right).

C. Northern blot analysis showing transcription of *rom4::mCherry*. Hybridization was performed using a PCR probe recognizing the *rom4* gene (primers 6929/6930). As a loading control, hybridization was performed with probe L644R that recognizes the large subunit ribosomal RNA (see Table S3 for primer sequences and product sizes). wt, wild-type.

D. Immunofluorescence analyses of schizonts and gametocytes of *rom4::mCherry* using anti-mCherry antibody. Distinct mCherry staining was observed in gametocytes (gct) whereas in schizonts (schz) only weak signals (barely above background signals) were observed. Staining was performed using anti-mCherry (red) and anti-MSP1 (green) antibodies and the DNA dye Hoechst-33258 (blue). BF, bright field.

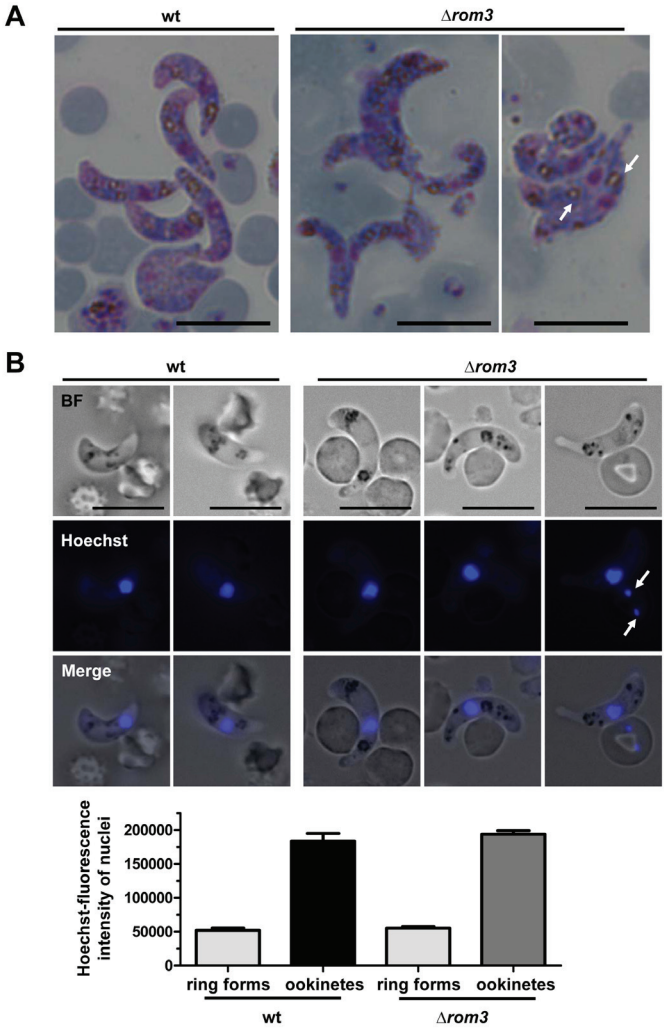

Figure S3. Morphology and nuclear DNA content of Δ*rom3* and wild type ookinetes analyzed by light and fluorescence microscopy.

A. Morphology of Giemsa stained *in vitro* cultured ookinetes. Δ*rom3* ookinetes have the characteristics of fully mature WT ookinetes such as an elongated 'banana' shape, hemozoin clusters (white arrows) and centrally located nucleus. Scale bar 10 µm.

B. Nuclear DNA content of Δ*rom3* and wild type live ookinetes as determined by Hoechst -fluorescence intensity measurements. The mean fluorescence intensity of haploid ring-form nuclei (white arrows) is 53632 (relative light intensity; RLI). The Δ*rom3* and wild type ookinetes show similar (tetraploid) DNA content and both have similarly enlarged nuclei, with RLI values of 193788 and 183668, respectively. BF: bright field. Scale bar 10 µm. Twenty parasites were measured and the means and SEM are shown in the graph, n=20.

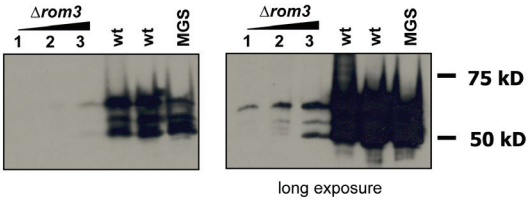

Figure S4. Circumsporozoite protein expression in Δ*rom3* and wild-type oocysts

Western blot analysis of proteins isolated from increasing numbers of midguts of Δ*rom3* infected mosquitoes. Midguts from mosquitoes infected with Δ*rom3* (1, 2 or 3 midguts, day 13) and wild-type (wt, day 13) were separated on SDS-PAGE and stained with anti-CS antibody. Purified 10^5 wt midgut sporozoites (MGS) were used as a control. Right hand panel shows a longer exposure of the blot on the left.

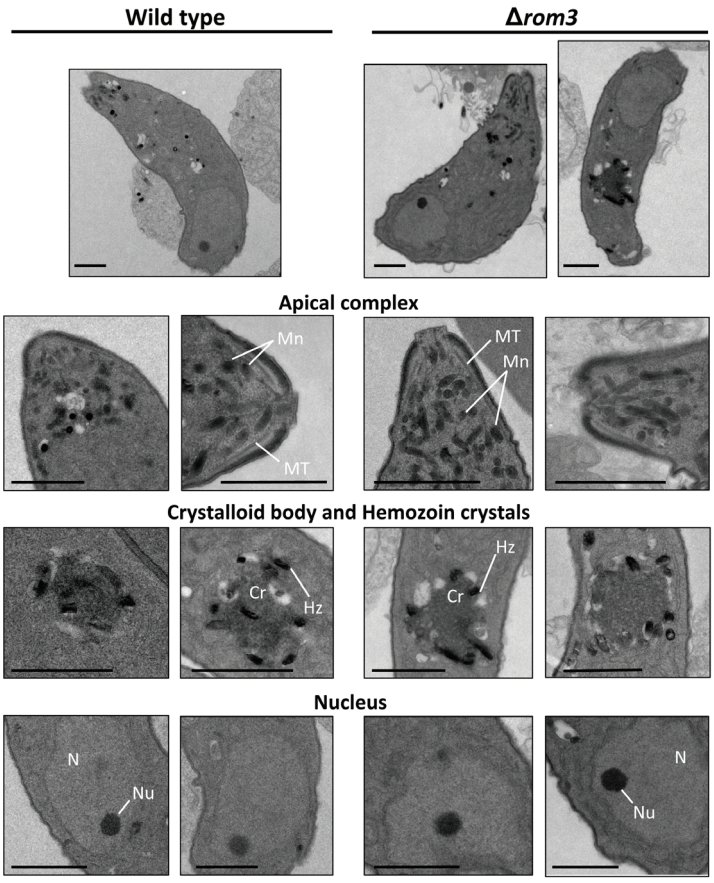

Figure S5. **Ultrastructural analyses of wt and Δ*rom3* ookinetes.**

Both wt and Δ*rom3* parasites produce normal ookinetes with respect to size, organelles and membrane morphology. No differences were observed in the apical complex which has a similar distribution and localization of micronemes (Mn), the arrangement of the subpellicular microtubules (MT), morphology of the crystalloid body (Cr) and hemozoin crystals (Hz). No differences were observed in the nucleus (N), the nuclear membrane, or in the nucleolus-like (Nu) structure between wt and Δ*rom3* ookinetes. Scale bar 1μM.

Table S1. Gene deletion experiments to disrupt the *P. berghei* genes encoding rhomboid proteases

Gene name, Gene deletion mutant	Gene ID	DNA construct name	Experiment No., Mutant name[1]	Parent line[2]	RMgmDB ID[3]
Unsussessful attempts					
rom4	PBANKA_110650	pL1078	653, 684, 695	cl15cy1	RMgm-187
rom6	PBANKA_135810	PCR1916	2118, 2119 2140	1037m1f1cl1 676m1cl1	RMgm-758
rom7	PBANKA_113460	PCR1917	2120, 2121 2141	1037m1f1cl1 676m1cl1	RMgm-759
rom8	PBANKA_103130	PCR1918	2122, 2123 2142	1037m1f1cl1 676m1cl1	RMgm-760
Mutants					
Δ*rom1*-p	PBANKA_093350	Mg031	538cl2	cl15cy1	RMgm-177
Δ*rom1*-c		pL1533	1496cl4	676m1cl1	RMgm-761
Δ*rom3*-a	PBANKA_070270	pL1097	430cl1	cl15cy1	RMgm-178
Δ*rom3*-b		pL1097	687cl1	cl15cy1	
Δ*rom9*-a	PBANKA_111470	PCR1919	2124cl1	1037m1f1cl1	RMgm-762
Δ*rom9*-b		PCR1919	2125cl1	1037m1f1cl1	
Δ*rom10*	PBANKA_111780	Mg011	468cl2	cl15cy1	RMgm-179
Fluorescence-tagged mutants					
rom3::gfp	PBANKA_070270	pL1079	654cl1	cl15cy1	RMgm-763
rom4::mCherry	PBANKA_110650	pL1920	2143cl1	676m1cl1	RMgm-764

[1] Experiment number for independent transfection experiments: the unsuccessful attempts (×3) and the experiment number/clone of the gene deletion mutants

[2] Parent *P. berghei* ANKA line in which the genes were targetted for deletion

[3] The ID number of the mutants (or of the unsuccessful attempts for gene deletion) in the RMgm database (www.pberghei.eu) of genetically modified rodent malaria parasites

Table S2. Targeting constructs and primers

Gene	Construct	Basic construct	No.	Sequences	Restriction sites	Description
Gene deletion constructs						
rom1	Mg031	pL0001	2082	AACAATTGATTCGTTGTGAATATAATCAGG	*Mun*I	5′- *rom1* targeting region F
			2083	TTAAGCTTGCATTCGGACACAATTAATAC	*Hind*III	5′- *rom1* targeting region R
			2086	AAGATATCAAGTTATAGTAAATATGCTTTGC	*EcoR*V	3′- *rom1* targeting region F
			2087	TTGGATCCCCTATGTATATATCTTTGTACCG	*BamH*I	3′- *rom1* targeting region R
	pL1533	pL0001	4718	GACGGGTACCTATCGAGCAACAATGTCTG	*Asp718*I	5′- *rom1* targeting region F
			4937	CCCATCGATAAATAAGTCCAAACTCAAAGC	*Cla*I	5′- *rom1* targeting region R
			4697	CCGGAATTCAAGTTATAGTAAATATGCTTTGC	*EcoR*I	3′- *rom1* targeting region F
			2087	TTGGATCCCCTATGTATATATCTTTGTACCG	*BamH*I	3′- *rom1* targeting region R
rom3	pL1097	pL0001	1754	AAATCGATGAATTCCAACAATGAATGTAATAAAGG	*Cla*I, *EcoR*I	5′- *rom3* targeting region F
			1755	TTAAGCTTATGTCTATTTTGTTTCACTTG	*Hind*III	5′- *rom3* targeting region R
			1756	AAGATATCAATTAAGTATATTAGGATAAC	*EcoR*V	3′- *rom3* targeting region F
			1757	TTGGATCCACGAAGCAAGTTATTGCACAC	*BamH*I	3′- *rom3* targeting region R
rom4	pL1078	pL0001	2408	AAAGAATTCTGCATGTATAAGTAATGTGC	*EcoR*I	5′- *rom4* targeting region F
			2409	AAAAAGCTTTCATTCAAGAGAGTTGGAAC	*Hind*III	5′- *rom4* targeting region R
			2410	AAAGATATCCAATTAATTGAAGAAAAGGC	*EcoR*V	3′- *rom4* targeting region F
			2411	AAAGGATCCTTTATTATCTTAAAATGCGC	*BamH*I	3′- *rom4* targeting region R
rom6	PCR1916	pL0048	7055	GAACTCGTACTCCTTGGTGACGTCGCGACTATTTTTTATAGGCACATTTTG	*Nru*I	5′- *rom6* targeting region F
		PCR	7056	CATCTACAAGCATCGTCGACCTCGTATAGCGTTTTTTTTACAATAGTG		5′- *rom6* targeting region R
			7057	CCTTCAATTTCGGATCCACTAGAAAAACATAACCACCATATGC		3′- *rom6* targeting region F
			7058	AGGTTGGTCATTGACACTCAGCTCGCGACATCCTGCTTTGCTATACC	*Nru*I	3′- *rom6* targeting region R
rom7	PCR1917	pL0048	7063	GAACTCGTACTCCTTGGTGACGTCGCGATGCTTTGTATTTTCATTGGAG	*Nru*I	5′- *rom7* targeting region F
		PCR	7064	CATCTACAAGCATCGTCGACCTCATGATGTCTCTTTGATATTATTC		5′- *rom7* targeting region R
			7065	CCTTCAATTTCGGATCCACTAGATGTCGTCCACATTAATTTTG		3′- *rom7* targeting region F
			7066	AGGTTGGTCATTGACACTCAGCTCGCGATTCCGAAGCATTACATAAGG	*Nru*I	3′- *rom7* targeting region R
rom8	PCR1918	pL0048	7071	GAACTCGTACTCCTTGGTGACGTCGCGAGTGAAGATTTTGAATAAATAGAAGAAG	*Nru*I	5′- *rom8* targeting region F
		PCR	7072	CATCTACAAGCATCGTCGACCTCATGCCAATTCACAAATAATGC		5′- *rom8* targeting region R
			7073	CCTTCAATTTCGGATCCACTAGATATGTGTATACTACCAGTATCC		3′- *rom8* targeting region F
			7074	AGGTTGGTCATTGACACTCAGCTCGCGATGCATTTCACAATAATTTTACAC	*Nru*I	3′- *rom8* targeting region R
rom9	PCR1919	pL0048	7079	GAACTCGTACTCCTTGGTGACGTCGCGAATAAGCGCATGTCATTTGTTG	*Nru*I	5′- *rom9* targeting region F
		PCR	7080	CATCTACAAGCATCGTCGACCTCGTAAGAATATGCTGGAATTGG		5′- *rom9* targeting region R

			7081	CCTTCAATTTCGGATCCACTAGCTCTAGTCTATATGAACATAAAACTC		3'- *rom9* targeting region F
			7082	AGGTTGGTCATTGACACTCAGCTCGCGATTTCAGCAATAGAAGAAACAAG	*Nru*I	3'- *rom9* targeting region R
rom10	Mg011	pL0001	1774	AAGGGCCCTCACATTTTCCCATCAGAG	*Apa*I	5'- *rom10* targeting region F
			1775	TTATCGATTCTGTCTATACATGCCCAAG	*Cla*I	5'- *rom10* targeting region R
			1776	AAGATATCCATACGTAATATGTCTATGC	*EcoR*V	3'- *rom10* targeting region F
			1777	TTGGATCCAGTTATAACTGCAGGTGTTC	*BamH*I	3'- *rom10* targeting region R
		anchor-tag primers				
			4661	GAACTCGTACTCCTTGGTGACG		anchor-tag primer, F
			4662	AGGTTGGTCATTGACACTCAGC		anchor-tag primer, R
C- terminal tagging constructs						
rom3	pL1079		1754	AAATCGATGAATTCCAACAATGAATGTAATAAAGG	*Cla*I	*rom3* ORF, F
			2415	AAAGGATCCAGCAAATTCACATGGCATATTC	*BamH*I	*rom3* ORF, R
rom4	pL1920	pL1646	7016	AGCACTAGTATGGAAACAAATAAACCGAAAAAGG	*Spe*I	*rom4* ORF, F
			7017	GGGAGATCTTTCCTTGCAATAATAATCAAATG	*Bgl*II	*rom4* ORF, R

Red: restriction sites
Blue: 5'- extensions homologues to the h*dhfr*::y*fcu* selectable marker cassette from pL0048
Green: 5'- extensions homologues to the anchor tag primers 4661/4662

Table S3. Primers for genotyping

Genes	No.	Primer sequences	Description	Integration PCR Pair	Product size (bp)
Primers for PCR analyses					
rom1	4586	TTATGCATTGTATAACATCTCTG	*rom1* 5′ in-F	695	1172
	5036	ACCATTATTTTTTGTATGTAGTG	*rom1* 5′ in-F	695	1138
	4587	CTGATGATATTATTAAGAGAACTG	*rom1* 3′ in-R	4239	998
	2084	TGGAAATATACTATCATCATCTG	*rom1* ORF-F		501
	2085	ACAGCAAACAAAACAACAGTTGG	*rom1* ORF-R		
rom3	2389	GGTATAATTTTGTTTATC	*rom3* 5′ in-F	695	867
	1886	CAACACTCTTGAAGGATGTC	*rom3* 3′ in-R	4239	1024
	1812	TTATTGTATGGATTAGTTTTTTCC	*rom3* ORF-F		787
	1813	TATCCCAAAAATTTGTTATAATGG	*rom3* ORF-R		
rom4	2451	AGTTAATTTATAAACATGC	*rom4* 5′ in-F	695	1015
	2452	CACACATATTTATCAGTGC	*rom4* 3′ in-R	4239	787
	6929	ATTGCATACATTGCCATCTG	*rom4* ORF-F		973
	6930	TAACATCCGTTCTCCTAATGTG	*rom4* ORF-R		
rom6	7059	CATATTTGTAATGCTCAAAATAGTG	*rom6* 5′ in-F	4906	1211
	7060	ACGAAAAGGAAAGAAAAGATAATTAG	*rom6* 3′ in-R	4239	1219
	7061	CCTTTTACCAAAGTGGTGAG	*rom6* ORF-F		1033
	7062	CACCTAAAAGTTGAGCATATCTG	*rom6* ORF-R		
rom7	7067	GAAGGGGAAATTATTTGATATATGG	*rom7* 5′ in-F	4906	1425
	7068	GTGACGATGAAAAATTTGATG	*rom7* 3′ in-R	4239	971
	7069	CGATTCAAAAAATATAATAATGTAGAG	*rom7* ORF-F		787
	7070	GGCTAACATTTTCTAAAAGTAGAG	*rom7* ORF-R		
rom8	7075	CCCCCCATTTTTTATTATTATTAAC	*rom8* 5′ in-F	4906	1364
	7076	GCTATAGAAAACGGGAAACATC	*rom8* 3′ in-R	4239	1061
	7077	TAAATGGCAGTAAAGAATATGAC	*rom8* ORF-F		940
	7078	TTCCGAAATAAAAAGCATCGTC	*rom8* ORF-R		
rom9	7083	AATACAAATTTCAGAGGATGAC	*rom9* 5′ in-F	4906	1242
	7084	AAATAGGAATAAAGTGAGTAAGC	*rom9* 3′ in-R	4239	940
	7085	GAATGAAATTTGTGGGTAAGG	*rom9* ORF-F		970
	7086	GTATTGTGACTTATTATGTTAGTTAC	*rom9* ORF-R		
rom10	6939	AGCAATATCTTATTTGCTACATAC	*rom10* 5′ in-F	4179	714
	2088	CATTATAGTACAATTATAGGTG	*rom10* 3′ in-R	4239	1093
	6940	CATAACTGCAACATTAATTCATC	*rom10* ORF-F		989
	2066	CCGATATTTCCCATAATGTTTC	*rom10* ORF-R		
Universal primers					
	695	AATATTCATAACACACTTTTAAGC	5′*pbdhfr*/*ts* R		
	4906	CGACTAGTTAATAAAGGGCAC	5′*pbeef1a* R		
	4179	CTATAGGGCGAATTGGAGCTC	*LacZ* R		
	4239	GATTTTTAAAATGTTTATAATATGATTAGC	3′*pbdhfr*/*ts* F		
	4598	GGACAGATTGAACATCGTCG	*tgdhfr*/*ts* F		1059
	4599	GTGTAGTCTGTGTGCATGTC	*tgdhfr*/*ts* R		
	4698	GTTCGCTAAACTGCATCGTC	h*dhfr* F		787
	4699	GTTTGAGGTAGCAAGTAGACG	y*fcu* R		

Other Primers for generation of probes

692	CGCGGATCCATGCATAAACCGGTGTGTC	3'*pbdhfr/ts* F
693	CGCGGATCCGCTAGACAGCCATCTCCAT	3'*pbdhfr/ts* R
741	CGCGGATCCATGCATAAACCGGTGTGTC	*tgdhfr/ts* F
742	CGCGGATCCGCTAGACAGCCATCTCCAT	*tgdhfr/ts* R
2082	AACAATTGATTCGTTGTGAATATAATCAGG	*rom1* upst F
L644R	GGAAACAGTCCATCTATAATTG	*lsu rrna* (A-type)

pb = P. berghei, *tg = T. gondii;* h = human, y = yeast

5' in=5' integration PCR; 3' in=3' integration PCR

Table S4. Primers for RT-PCR analyses

Gene	No.	Sequences	Description	Expected gDNA (bp)	Expected cDNA (bp)	Across intron
rom1	2084	TGGAAATATACTATCATCATCTG	*rom1* ORF-F	501	368	yes
	2085	ACAGCAAACAAAACAACAGTTGG	*rom1* ORF-R			
rom3	1812	TTATTGTATGGATTAGTTTTTTCC	*rom3* ORF-F	787	562	yes
	1813	TATCCCAAAAATTTGTTATAATGG	*rom3* ORF-R			
rom4	42	AAATCTAGAGACAAAGGTCGATTAG	*rom4* ORF-F	510	510	no
	43	AAACCGCGGAGCATATCCTCGACCATC	*rom4* ORF-R			
rom6	470	GGGGAATTCCATTGGCGGG	*rom6* ORF-F	506	506	no
	7062	CACTAAAAGTTGAGCATATCTG	*rom6* ORF-R			
rom7	7069	CGATTCAAAAAATATAATAATGTAGAG	*rom7* ORF-F	787	787	no
	7070	GGCTAACATTTTCTAAAAGTAGAG	*rom7* ORF-R			
rom8	7408	TAATTATACACCACCTGAAAATG	*rom8* ORF-F	922	529	yes
	7409	CGATGAACTACTACTACTTTCTG	*rom8* ORF-R			
rom9	1107	AAACAATTGTTTACTAAATACAATTTC	*rom9* ORF-F	730	408	yes
	1108	TATTCGAAACTTTTTATTAAC	*rom9* ORF-R			
rom10	6940	CATAACTGCAACATTAATTCATC	*rom10* ORF-F	989	363	yes
	2066	CCGATATTTCCCATAATGTTTC	*rom10* ORF-R			

Table S5. Potential substrates of ROM3; *P. berghei* single transmembrane domain containing oocyst and sporozoite proteins

Gene ID (*P. berghei*)	Gene ID (*P. falciparum*)	# Unique Peptides[1]	# of Spectra[1]	Product Description	# TM Domains	SignalP Peptide	Deletion Attempted (RMgmDB[2] #)	Phenotype[2]
PBANKA_091500	PF3D7_1133400	2	4	apical membrane antigen 1 (AMA1)	1	HMM: MRKLYCVLLLSAFEFTYMINFGRGQ, NN: MRKLYCVLLLSAFEFTYMINFGRGQ	Yes (10)	Not possible to KO
PBANKA_100360	PF3D7_0405900	5	25	apical sushi protein (ASP)	1	HMM: MKIIYHILIFLLHYNIIIKAK, NN: MKIIYHILIFLLHYNIIIKAK	No	
PBANKA_081340	PF3D7_0912400	7	49	conserved *Plasmodium* protein, unknown function	1	HMM: MNTCIKLIFAFFIFIKYGRCQ, NN: MNTCIKLIFAFFIFIKYGRCQ	No	
PBANKA_094160	PF3D7_1105300	4	16	conserved *Plasmodium* protein, unknown function	1	HMM: MRKIIPLLYSVIIFFVFKSWSY, NN: MRKIIPLLYSVIIFFVFKSWSY	No	
PBANKA_081150	PF3D7_0910300	2	4	conserved *Plasmodium* protein, unknown function	1	HMM: MIFLRNGFFFLFSVLTSCYINLFTQCLGE, NN: MIFLRNGFFFLFSVLTSCYINLFTQCLGE	No	
PBANKA_144390	PF3D7_1229300	1	1	conserved *Plasmodium* protein, unknown function	1	HMM: MKLKYHLFFLIIFIQDILCL, NN: MKLKYHLFFLIIFIQDILCL	No	
PBANKA_090130.1	PF3D7_1147800.1	33	1089	merozoite adhesive erythrocytic binding protein (MAEBL)	1	HMM: MGVLKHFFFLLFLYVNNTSAI, NN: MGVLKHFFFLLFLYVNNTSAI	Yes (220)	Important for sporozoite invasion of Salivary gands
PBANKA_020920	PF3D7_0103900	5	25	parasite-infected erythrocyte surface protein (PIEPS15)	1	HMM: MRKTKGRLVFYLCISIWCLFVNICK, NN: MRKTKGRLVFYLCISIWCLFVNICK	Yes (90)	No clear phenotype, no phenotype in mosquito
PBANKA_131570	PF3D7_1452000	12	144	rhoptry neck protein 2 (RON2)	1	HMM: MLKFFIFILHIYLYIDSIYSS, NN: MLKFFIFILHIYLYIDSIYSS	Yes (214)	Not possible to KO
PBANKA_020910	PF3D7_0104000	1	1	thrombospondin-related sporozoite protein (TRSP)	1	HMM: MLMKISRYFFLLYLIKAHLD, NN: MLMKISRYFFLLYLIKAH	Yes (34)	Normal salivary gland sporozoite (SGS) numbers but hepatocyte invasion reduced
PBANKA_130650	PF3D7_1442600	20	400	TRAP-like protein, sporozoite-specific transmembrane protein S6 (TREP)	1	HMM: MNFFSIFIILNFFMLSLTSSLGN, NN: MNFFSIFIILNFFMLSLTSSLGN	Yes (145/159/305)	Normal oocyst derived sporozoite (ODS) numbers, but reduced SGS numbers; reduced motility of ODS

[1] Based on Lasonder E *et al*. 2008 PLoS Pathogens 4(10): e1000195

[2] Data on attempted and successful deletions of these genes available from the RMgm Database (database entry www.pberghei.eu)